Correlation and relativistic effects in U metal and U-Zr alloy: Validation of *ab initio* approaches

Wei Xie (谢玮),[1,*] Wei Xiong,[2] Chris A. Marianetti,[3] and Dane Morgan[1,2,4,†]

[1]*Materials Science Program, University of Wisconsin-Madison, Madison, Wisconsin 53706, USA*

[2]*Department of Materials Science and Engineering, University of Wisconsin-Madison, Madison, Wisconsin 53706, USA*

[3]*Department of Applied Physics and Applied Mathematics, Columbia University, New York, New York 10027, USA*

[4]*Department of Engineering Physics, University of Wisconsin-Madison, Madison, Wisconsin 53706, USA*

(Received 21 June 2013; published 26 December 2013)

Ab initio calculations have been performed on all solid phases of U metal and U-Zr alloy, the basis of a promising metallic fuel for fast nuclear reactors. Based on generalized gradient approximation, both density functional theory (DFT) in its standard form and the so-called DFT plus Hubbard U (DFT + U) modification are evaluated. The evolution of calculated energetics, volume, magnetic moments, electronic structure, and f-orbital occupation as functions of the effective Hubbard U parameter, U_{eff}, is carefully examined at U_{eff} from 0 to 4 eV. DFT is found to overestimate energetics, underestimate volume, downward shift some f bands near Fermi level and overestimate f-orbital occupation against existing experimental and/or computational data. The error is ∼0.07 eV/atom in terms of enthalpy, which affects phase stability modeling for δ(U,Zr) and γ(U,Zr). DFT + U at $U_{\text{eff}} = 1-1.5$ eV offers clear improvement on these calculated properties (∼0.05 eV/atom in terms of enthalpy) and in general still neither promotes ordered magnetic moments nor opens unphysical band gaps, which occur at higher U_{eff} values. The empirical U_{eff} values of 1–1.5 eV are close to but smaller than the theoretical estimations of 1.9–2.3 eV that we obtain from the linear response approach. U_{eff} is found to vary only slightly ($\leqslant$0.24 eV) between different phases and at different compositions of U and U-Zr; thus, a single $U_{\text{eff}} = 1.24$ eV, which is the statistical optimal from energetic fitting, is suggested for both U and U-Zr. Besides correlation, the relativistic effect of spin-orbit coupling (SOC) is also systematically explored. SOC is found to lower energy, increase volume, and split the 5f shell above Fermi level and reduce f-orbital occupation. The effect predominates in the unoccupied states and is very small on all these calculated ground state properties (∼0.02 eV/atom in terms of enthalpy).

DOI: 10.1103/PhysRevB.88.235128 PACS number(s): 31.15.A−, 31.15.E−, 31.15.V−

I. INTRODUCTION

U-Pu-Zr-M (M = minor actinides Np, Am, Cm) alloy is a promising metallic fuel for fast nuclear reactors with advantages in thermal conductivity, burn-up, recycling, and other factors.[1] Its safety and efficiency are nevertheless affected by issues like constituent redistribution and fuel swelling, which are closely related to its phase stability. Better modeling of the phase stability will help improve the design and guide the safe and optimal use of this fuel, and model validation is important toward this objective. U metal and U-Zr alloy are the primary constituents of this multicomponent fuel, have most experimental and computational data available,[2–6] and hence are ideal systems for validating *ab initio* approaches.

Many density functional theory[7,8] (DFT)–based *ab initio* calculations of U metal have been reported[9–25] since the 1970s. An important conclusion of some early studies[10,12] is that for U metal, generalized gradient approximation (GGA)[26] improves local density approximation (LDA)[8] to the exchange-correlation functional, with which the calculated structural and elastic properties reproduce experimental data quite well. However, how accurate GGA can calculate the total energy is less certain due to the lack of direct experimental thermochemical data for validation. Moreover, βU is often neglected and has been calculated only recently.[20,25] Different from U metal, U-Zr alloy has just been explored in *ab initio* studies[27–30] recently. Landa *et al.*[27] calculated the body-centered-cubic (bcc) solution phase γ(U,Zr) with the Korringa-Kohn-Rostoker method in the atomic sphere approximation (KKRASA). The resulted enthalpy of mixing is very close to that from their own full-potential linear muffin-tin orbitals (FPLMTO) calculations and a previous CALculation of PHase Diagrams (CALPHAD) model.[31] Interfacing with Monte Carlo simulation and adding phonon contribution, they further calculated its decomposition temperature, which is about 350 K higher than the experimental miscibility gap. Besides γ(U,Zr), they also confirmed the partial ordering of the intermediate phase δ(U,Zr) with the exact muffin-tin orbital (EMTO) method and explained its existence in the U-Zr system using d-orbital occupation change relative to ωZr. Other studies[28–30] used the projector-augmented wave (PAW) method. Huang and Wirth[28,29] calculated the defect formation energy and migration barriers in α(U). Basak *et al.*[30] obtained the energy difference between γ(U,Zr) and δ(U,Zr) at 66.7 at.% Zr to be 4.87 kJ/mol. As far as we are aware, previous calculations of U-Zr alloy have not treated the terminal solution phases β(U) and α(Zr), and the accuracy of calculated energetics is just starting to be assessed.

In general, when studying actinide systems, it is important to understand the extent of and validate modeling approaches on correlation and relativistic effects. Here we briefly summarize recent experimental and computational studies of these effects in U metal. Opeil *et al.*[32,33] compared the density of states (DOS) and band structure calculated from DFT-GGA to their experimental photoemission spectra and band energy dispersion intensity map of an αU single crystal. They found that, overall, the experimental spectral characteristics are reproduced; however, one of the calculated DOS peaks and several f bands just below Fermi level are shifted downward

with respect to measured spectra. Going beyond LDA/GGA, Chantis *et al.*[34] calculated the electronic structure of αU with the many-body quasiparticle self-consistent GW (QSGW) method. They found that, compared to DFT-LDA, f band from QSGW is shifted with respect to the remaining metallic bands by about 0.5 eV and significantly narrower leading to a smaller f-orbital occupation. They concluded that the correlations predominate in the unoccupied part of the f states and explain that LDA/GGA can reproduce the structural and elastic properties of U metal well because of the overall low f-orbital occupation. However LDA/GGA still misplaces several bands just below Fermi level and overestimates f-orbital occupation, which may have more pronounced effects on other properties like energetics, the accuracy of which has not been systematically tested yet. Regarding the relativistic effects, Soderlind[16] found that spin-orbit coupling (SOC) mainly changes the unoccupied part of the density of states for αU and explained that its effect on calculated properties is not large again due to the relatively small f-orbital occupation. Alloying with Zr further complicates the situation because Zr may change the f-orbital occupation and promote both correlation and relativistic effects, as in many heavy fermion U intermetallics.[35] However, previous *ab initio* studies[27–30] of U-Zr have not tested any beyond the DFT approach and have neglected SOC, to the best of our knowledge.

Summarizing existing literature, several important questions remain open: How accurate can DFT based on LDA/GGA alone calculate energetics for U and U-Zr? How much better can we get, going beyond them? To answer these questions, we validate, on the basis of GGA, the standard DFT, as well as beyond the DFT functional DFT + U[36] in this study. DFT + U has shown success on many U intermetallic alloys. For example, DFT + U could reproduce the magnetic moments of UGe_2 that is underestimated by DFT based on LDA.[37] It also in general gives better calculated x-ray magnetic circular dichroism (XMCD) spectra for UX_3 (X = Pd, and Pt),[38,39] UFe_2,[40] UBe_{13},[39] UTAl (T = Co, Rh, and Pt),[41] and UT_2Al_3 (T = Ni and Pd),[39] relative to DFT-LDA. It is therefore interesting to see whether similar improvement also exists on U-Zr. For U metal, there is an initial evaluation of DFT + U on αU.[42] However, merely two U_{eff} points at 0.5 and 3 eV are tried for the αU phase only. A more systematic study covering broader U_{eff} range for all solid phases would be favored. Moreover, if DFT + U turns out to be a good model for U and U-Zr, what Hubbard U parameters to use for them is also unsettled. Previous studies use $U = 0.7$ and $J = 0.44$ eV for UGe_2 (Ref. 37) and $U = 2$ and $J = 0.5$ eV for the many systems studied in Refs. 38–41. It is unclear whether such values are reasonable for U and U-Zr as well. Therefore, we also seek to determine them in terms of their effective value $U_{\text{eff}} = U - J$ for U and U-Zr in this study.

In this paper, we look at *all* solid phases of both U and U-Zr. Based on GGA, we validate both the standard DFT and the DFT + U functionals at a wide range of U_{eff} from 0 to 4 eV and explore the effect of SOC in terms of calculated energetics, volume, magnetic moments, electronic structure, and f-orbital occupation. The accuracy of calculated energetics is determined by comparing them with best established thermodynamic models, in addition to available experiments. The Hubbard U parameters for U metal and U-Zr alloy are determined both empirically by fitting to existing experimental and/or computational data and theoretically by using the linear response approach.[43]

This manuscript proceeds as follows. Section II describes the computational details, including materials systems, *ab initio* methods and parameters, definitions of energetics, and approximations adopted and their justifications. In Sec. III, the evolution of energetics, volume, magnetic moments, electronic structure, and f-orbital occupation as functions of U_{eff} is examined from $U_{\text{eff}} = 0$–4 eV in calculations both with and without SOC included. The empirically fitted U_{eff} is compared to theoretically calculated Hubbard U values, and suggestions are given on choosing U_{eff} for U and U-Zr. Finally, Sec. IV summarizes the conclusions of this study.

II. COMPUTATIONAL DETAILS

All solid phases of U metal, Zr metal, and U-Zr alloy, as summarized in Table I, are calculated in this study.

TABLE I. Solid phases of U, Zr metal, and U-Zr alloy.

Phase[a]	Structure name	Space group	Composition (at.% Zr)	Cell size (atoms/cell)	SQS used?	k-Point mesh	Expt. refs.
αU	Orthorhombic_A20	$Cmcm$	0	2	No	$8 \times 8 \times 8$	Ref. 44
α(U)			6.3	16	Yes	$5 \times 5 \times 5$	
βU	Tetragonal_A_b	$P4_2/mnm$	0	30	No	$3 \times 3 \times 6$	Ref. 45
β(U)			3.3	30	Yes	$3 \times 3 \times 6$	
γU			0	1	No	$17 \times 17 \times 17$	Ref. 46
			6.3				
			25.0				
γ(U,Zr)	Bcc_A2	$Im\bar{3}m$	50.0	16	Yes	$6 \times 6 \times 6$	Ref. 50
			75.0				
			93.8				
βZr			100	1	No	$17 \times 17 \times 17$	Ref. 49
δ(U,Zr)	Hexagonal_C32	$P6/mmm$	66.7	12	Yes	$9 \times 9 \times 9$	Ref. 51
ωZr			100	3	No	$9 \times 9 \times 13$	Ref. 48
α(Zr)	Hcp_A3	$P6_3/mmc$	93.8	16	Yes	$4 \times 4 \times 4$	Ref. 47
αZr			100	2	No	$8 \times 8 \times 8$	

[a]A phase is elemental/alloyed when labeled without/with parentheses.

Zr metal is not the main object of this study but is also calculated to serve as an end member reference. Elemental U and Zr metal phases, that is, αU, βU, γU, αZr, ωZr, and βZr, are modeled using their primitive unit cells.[44–49] U-Zr alloy phases, that is, α(U), β(U), α(Zr), γ(U,Zr), and δ(U,Zr), all have certain structural disorder and thus are modeled using supercells that are generated based on their experimental crystal structures[44,45,47,50,51] using the special quasirandom structure (SQS) method[52] as implemented in the Alloy Theoretic Automated Toolkit.[53] First, the terminal solution phases α(U), β(U), and α(Zr) are studied with one solute atom in supercells of 16, 30, and 16 atoms, respectively. The solute concentrations have exceeded the solubility limit, but we believe they are acceptable model systems to probe the dilute alloying effect because the solute atoms are at least 5.2, 5.6, and 7.7 Å apart in these cells, respectively. Second, the single–solution phase bcc γ(U,Zr) is studied by five 16-atom supercells with composition 6.3, 25.0, 50.0, 75.0, and 93.8 at.% Zr (i.e., 1, 4, 8, 12, and 15 Zr atoms in supercells of 16 atoms), respectively. Among them, the three at 25.0, 50.0, and 75.0 at.% Zr are exactly those recommended by Jiang *et al.*[54] The other two at 6.3 and 93.8 at.% Zr are generated and selected in the same spirit. The 16-atom supercell has already been found to reach energy convergence.[54] Finally, the only intermediate-phase δ(U,Zr) has crystal structure of C32 (Ref. 51) in the Strukturbericht designation, which is isomorphous with ωZr.[48] More specifically, it has two distinct Wyckoff sites—site A has Wyckoff symbol 1*a* and coordinate (0, 0, 0), and site B has symbol 2*d* and coordinate (1/3, 2/3, 1/2). The occupation is 100 at.% Zr on site A and approximately 50 to 70 at.% Zr on site B. Here, we calculate a representative structure with 50 at.% Zr occupation on site B with overall chemical formula UZr_2. We find that the 12-atom supercell already converges the energy; therefore, a 12-atom SQS supercell structure is selected and used in this study.

All calculations are performed in the general framework of DFT[7,8] using the Vienna *Ab initio* Simulation Package (VASP).[55,56] The electron-ion interaction is described with the PAW method[57] as implemented by Kresse and Joubert.[58] The PAW potentials used treat $6s^2 6p^6 7s^2 5f^3 6d^1$ and $4s^2 4p^6 5s^2 4d^2$ as valence electrons for U and Zr, respectively. The exchange correlation functional parameterized in the GGA[26] by Perdew, Burke, and Ernzerhof (PBE)[59] is used. The stopping criteria for self-consistent loops used are 0.1 meV and 1 meV tolerance of total free energy for the electronic and ionic relaxation, respectively. We do not explicitly set force as a stopping criterion, but when the total free energy is converged according to the criteria above, the Hellmann-Feynman forces on atoms are generally <0.1 eV/Å or smaller. A cutoff energy of 450 eV is used throughout all calculations. The Brillouin zone is sampled with Monkhorst-Pack[60] *k*-point meshes given in Table I. We have tested that such *k*-point meshes and cutoff energy converge the total energy at least to 3 meV/atom, most even to 1 meV/atom. The partial occupancies are set using the Methfessel-Paxton method[61] of order 1 with a smearing width of 0.2 eV. All calculations have included spin polarization.

DFT as a theory is exact, but the exchange-correlation functional such as GGA used in this study is approximate. We hereinafter refer to the standard DFT functional and the DFT + U[36] functional simply as DFT and DFT + U, respectively. When we "compare" DFT and DFT + U below, it is important to remember that we are only comparing the two functionals based on GGA, not the two theories that are usually referred to under the same acronyms.

DFT + U[36] is an effective action theory that uses a functional of both the spin density, as in DFT, and the local spin-density matrix of some correlated subspace. The correlated subspace is typically defined using local, atomic-like orbitals as basis sets, and in this work, we use the standard implementation[62] in VASP. The screened interactions for these orbitals must be determined (i.e., U and J), and then the local interaction potential for this subspace is constructed within Hartree-Fock formalism. Given that one typically uses standard approximations (i.e., LDA/GGA) for the density-dependent potential, a double-counting correction must be used to remove the local correlations that are already present in LDA/GGA, and in this work, we use the standard fully localized limit double-counting correction.[63] Following Dudarev *et al.*,[64] we use a version of the DFT + U functional that does not introduce the explicit local exchange term J and is dependent on the effective value of $U_{\text{eff}} = U - J$. The functional recovers DFT exactly at $U_{\text{eff}} = 0$. This practice should be justified given that we are using a spin-density functional that already contains the effects of local exchange. Note that VASP still needs separate input of the U and J parameters, even though only $U_{\text{eff}} = U - J$ is used. For historical reasons, we do not set J to 0, but to 0.51 eV instead and vary U from 0.51 to 4.5 eV. Therefore, U_{eff} spans 0 and 4 eV (strictly, 3.99 eV). The Hubbard U potential is applied only on U sites for U metal and U-Zr alloys and is not used at all for elemental Zr metal.

The additional local spin-density matrix in the DFT + U functional introduces vast spin and orbital degrees of freedom, which pose a significant challenge to numerical optimization algorithms and often result in metastable solutions. We frequently encounter such problem in our systems. To avoid the metastable solution, Dorado *et al.*[65] suggested performing a manual combinatorial search for the ground state orbital configuration and impose it afterward. We cannot afford such a search here due to the large number of systems and U_{eff} points we pursue. Alternatively, Meredig *et al.*[66] proposed in the U-ramping method performing a series of calculations starting from DFT and extending adiabatically toward the point at the desired U_{eff}, with each step initializing from the charge density and relaxed structure of its previous one. We find that the original approach of Meredig *et al.*[66] cannot always guarantee a low-energy solution for our systems. In general, calculated properties of our systems are smooth functions of U_{eff} that have a clear three-stage pattern, as detailed in Sec. III. Metastable solutions are quite easy to identify as they break the pattern. Take αU as an example. We find that DFT correctly reproduces its experimental paramagnetic structure.[67,68] DFT + U promotes spin, and orbital polarization, which are still quenched at small U_{eff} by kinetic energy but will eventually overcome it after U_{eff}, is larger than a critical value. So the ground state solutions of DFT + U to αU should have zero magnetic moments at small U_{eff} until a critical point, after which moments emerge. Metastable solutions are characterized by wrong magnetic moments. If we follow the original proposal of Meredig *et al.*[66] to do U-ramping starting from DFT (i.e.,

$U_{\text{eff}} = 0$), we obtain solutions without moments, even when U_{eff} is larger than 2.5 eV, which has passed the critical U_{eff} and should have moments. On the other hand, if we do reverse U-ramping starting from large U_{eff} (large enough to promote net polarization, e.g., 4 eV for U and U-Zr) and gradually reduce U_{eff}, we always obtain solutions with large moments, even when U_{eff} is smaller than 1.5 eV, which has passed the critical U_{eff} and should have no or small moments. Fortunately, low-energy solutions are usually successfully obtained from the first series below 1.5 eV and from the second series above 2.5 eV. The problem lies within a critical region of 1.5–2.5 eV, for which the solutions from the two series, although they have very different magnetic moments, are very similar in energy. We thus have to manually select the low-energy solution from the two series in the critical region between 1.5 and 2.5 eV. With such care and efforts, we should have removed most metastable solutions in this study.

To compare with the U_{eff} from empirical fitting, we implement the linear response approach proposed by Cococcioni and de Gironcoli[43] in VASP and theoretically evaluate Hubbard U for U (ranium) in both the U metal and U-Zr alloy with self-consistent calculations described in the following. For elemental phases αU, βU, and γU, $2 \times 2 \times 2$, $1 \times 1 \times 1$, and $3 \times 3 \times 3$ supercells of their primitive cells that have 16, 30, and 27 atoms with Monkhorst-Pack k-point meshes of $6 \times 6 \times 4$, $3 \times 3 \times 6$, and $5 \times 5 \times 5$, respectively are used. For alloyed phases α(U), β(U), α(Zr), δ(U,Zr), and γ(U,Zr), the same supercells and k-point meshes given in Table I are used. All other numerical details are also the same as given above. Localized potential perturbations of -0.1, -0.05, 0, 0.05, and 0.1 eV are applied on a symmetrically distinct U atomic site (called a Hubbard site) to build the full response matrix and ultimately calculate U_{eff} following the procedures outlined in Ref. 43.

Regarding the relativistic effects, VASP always includes the mass-velocity and Darwin corrections using the methods proposed in Refs. 69 and 70 and thus all of our calculations are at least so-called scalar-relativistic. In more accurate calculations, we have included the effect of SOC in the LS-coupling limit. For convenience, in this paper we designate calculations as SOC and noSOC, respectively, for those with and without SOC included. SOC uses quantization axis (0, 0, 1) (i.e., z axis), starts with the charge density from noSOC, and relaxes both the magnitude and the direction of the magnetic moments self-consistently. All noSOC calculations treat magnetism collinearly and SOC noncollinearly, with one exception: When evaluating the band structure of αU, noSOC calculations also treat magnetism noncollinearly to avoid a bug that corrupts the calculated band structure.

We define the enthalpy of formation for any U and U-Zr phase as $E^{\text{form}}_{\text{U}_{1-x}\text{Zr}_x} = E^0_{\text{U}_{1-x}\text{Zr}_x} - (1-x)E^0_{\alpha\text{U}} - xE^0_{\alpha\text{Zr}}$, where $\text{U}_{1-x}\text{Zr}_x$ is the chemical formula, x is the mole fraction of Zr with $0 \leqslant x \leqslant 1$, and $E^0_{\text{U}_{1-x}\text{Zr}_x}$, $E^0_{\alpha\text{U}}$, $xE^0_{\alpha\text{Zr}}$ are the calculated total energy per atom for $\text{U}_{1-x}\text{Zr}_x$ and the two references αU and αZr at 0 K, respectively. For elemental phases, enthalpy of formation defined here is essentially what the CALPHAD community refers to as lattice stability. Similarly, we define the enthalpy of mixing specifically for the solution phase γ(U,Zr) as $E^{\text{mix}}_{\text{U}_{1-x}\text{Zr}_x} = E^0_{\text{U}_{1-x}\text{Zr}_x} - (1-x)E^0_{\gamma\text{U}} - xE^0_{\beta\text{Zr}}$, for which γU and βZr are used as the references. The two enthalpies can be straightforwardly converted to each other using the energetic differences between the two sets of references. Besides, the cohesive energies of the two ground state phases αU and αZr are also calculated with reference to the U and Zr atoms, respectively. They are each modeled in their respective atomic ground state with a simple cubic cell of 14 Å using a Γ point–only k-point mesh.

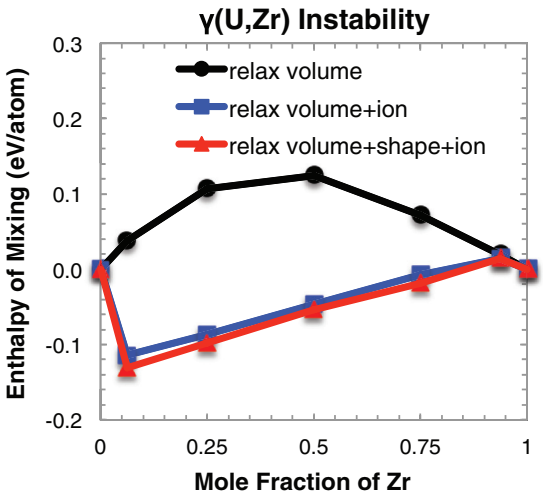

FIG. 1. (Color online) Enthalpy of mixing for γ(U,Zr) calculated from DFT-noSOC with different degrees of structural relaxations.

All calculations have relaxed all structural degrees of freedom—volume, ion position, and cell shape—for all phases except γU and γ(U,Zr), which are only volume-relaxed. γU has been proved to be strongly mechanically unstable at low temperatures.[6,71] Indeed, we find that fully relaxing even its one-atom primitive cell may collapse γU's cell shape from bcc, especially in SOC calculations. We could not find γ(U,Zr)'s structural instability documented in the literature, nor have we performed any elastic constants or phonon dispersion calculations for it, as was done in Refs. 6 and 71 for γU, but we suggest that γ(U,Zr) should also be mechanically unstable based on the following evidence. As shown in Fig. 1, the enthalpy of mixing for γ(U,Zr) is significantly negative as long as we allow the ion positions to relax, especially on the U-rich end, which is in contradiction to the existence of a miscibility gap for γ(U,Zr); examining the relaxed structures, ions displace significantly from the vicinities of bcc superlattice sites and approach those of βU, resulting in quasi-β(U) solution structures; the similar is true if we only relax cell shape, although the extent is small because these SQS supercells are already of very low symmetry (monoclinic or triclinic). To mitigate the strong mechanical instability in our 0 K calculations, we follow the practices of the previous calculations[16,27] and perform only volume relaxation for γU and γ(U,Zr). Such practice is physical for γU because it has no ion position or cell shape degree of freedom in the one-atom primitive bcc cell that we use. For γ(U,Zr), not relaxing the lattice should also only have minimal effect because these low-symmetry SQS supercells have no internal structural degree of freedom, which is demonstrated by the closeness between the enthalpies from volume + shape and volume + shape + ion relaxed calculations in Fig. 1. However, the lacking of ion relaxation for γ(U,Zr) sounds unsettling because ions need to be relaxed to accommodate the size mismatch

between U and Zr. Nevertheless, the radius of U and Zr atom is 1.56 and 1.60 Å in U and Zr metal,[72] respectively, differing only by 2.5%. In γ(U,Zr), Huber and Ansari[50] suggest that the size of the U and Zr atoms should also be comparable based on their lattice constant measurements. As a result, such constrained relaxation should only introduce trivial error due to the small size mismatch between U and Zr. However, it may still entangle with the differences between DFT and DFT + U and between noSOC and SOC, which are our main objects of model validation. Therefore, we should next put less weight on γ(U,Zr) than other phases.

We do not include finite temperature effects and focus only on exploring relativistic and correlation effects in this study, which is a reasonable and necessary first step for including them in future model validation. As a result, our calculated energetics are for 0 K, and corresponding experimental data—the most common standard for model validation—are mostly not available. A common approach to mitigate this problem is to extrapolate experimental energetics using thermodynamic models, such as those developed with the CALPHAD method.[73] The extrapolations in CALPHAD models are generally most reliable only at room temperature and above, and it is commonly assumed that energetics do not change much from 0 to 300 K. Therefore, here we choose enthalpies at 300 K from three recent CALPHAD models[74–76] of U-Zr and the Scientific Group Thermodata Europe (SGTE) database for pure elements[77] to validate our *ab initio* energetics. Relevant experimental data[78,79] are also used. The comparability between CALPHAD and *ab initio* energetics is still debatable due to temperature difference and issues like mechanical instability.[80–82] Our premise is that we consider all solid phases of U and U-Zr in this study, and if we obtain statistically significant results on energetics that are also consistent with other properties like electronic structure, the conclusion should be robust.

III. RESULTS AND DISCUSSION

The enthalpies of formation for all solid phases of U metal and U-Zr alloy except γ(U,Zr) are plotted in Figs. 2 and 3, respectively. αU is used as a reference when calculating the enthalpies, so its cohesive energy is given instead. A major observation is that DFT (i.e., $U_{\text{eff}} = 0$ eV) overestimates the energetics considerably for all the systems calculated here. The deviation is over 0.8 eV/atom for cohesive energy of αU and mostly over 0.05 eV/atom for enthalpy of formation of other phases. (The values are given in Table II and their statistics in Table III.) Particularly for δ(U,Zr), which is stable at low temperature and therefore should have negative or at most marginally positive enthalpy of formation at 0 K, the DFT calculation gives a considerably positive enthalpy of formation, 0.043 eV/atom, while CALPHAD models gave -0.013,[74] -0.045,[75] and 0 eV/atom,[76] and an available calorimetry experiment[78] gave -0.04 ± 0.11 eV/atom (-4.0 ± 10.1 kJ/mol). Our DFT result is, however, significantly different from that of Landa *et al.*[27] at -0.065 eV/atom, which is quite negative. We give a detailed analysis of the discrepancy here. The key differences between the *ab initio* approach of Landa *et al.*[27] and ours are (1) method to treat the disordered B site—we use SQS and they use the Coherent Potential Approximation (CPA), and (2) basis sets and potential—we use PAW and they use EMTO, although neither PAW nor EMTO is a strictly full potential method. The first difference (i.e., CPA vs SQS) can probably be ruled out as a source of large discrepancy because, as we will show later, our DFT calculations using PAW-SQS reproduce well the enthalpy of mixing for γ(U,Zr) from KKRASA-CPA calculations of Landa *et al.*,[27] which is also very close to their FPLMTO-SQS calculations. Now consider the second difference (EMTO vs PAW). PAW is fully capable of modeling both U and U-Zr. For U metal, PAW was shown in a number of previous studies[19–21] to reproduce its structural and elastic properties

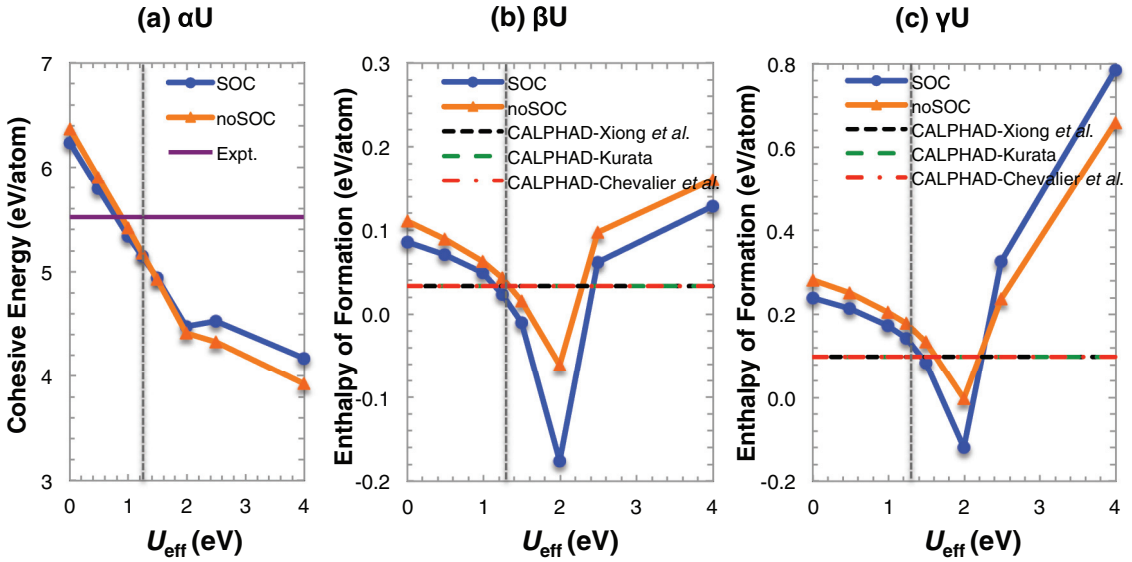

FIG. 2. (Color online) Energetics for U metal: (a) cohesive energy for αU; enthalpy of formation for (b) βU and (c) γU. The vertical dashed reference line is at $U_{\text{eff}} = 1.24$ eV. Experimental cohesive energy of αU is from Ref. 72; CALPHAD models are from Xiong *et al.*,[74] Kurata,[75] and Chevalier *et al.*,[76] which all use the same SGTE data for pure elements[77] and give the same enthalpy of formation for βU and γU.

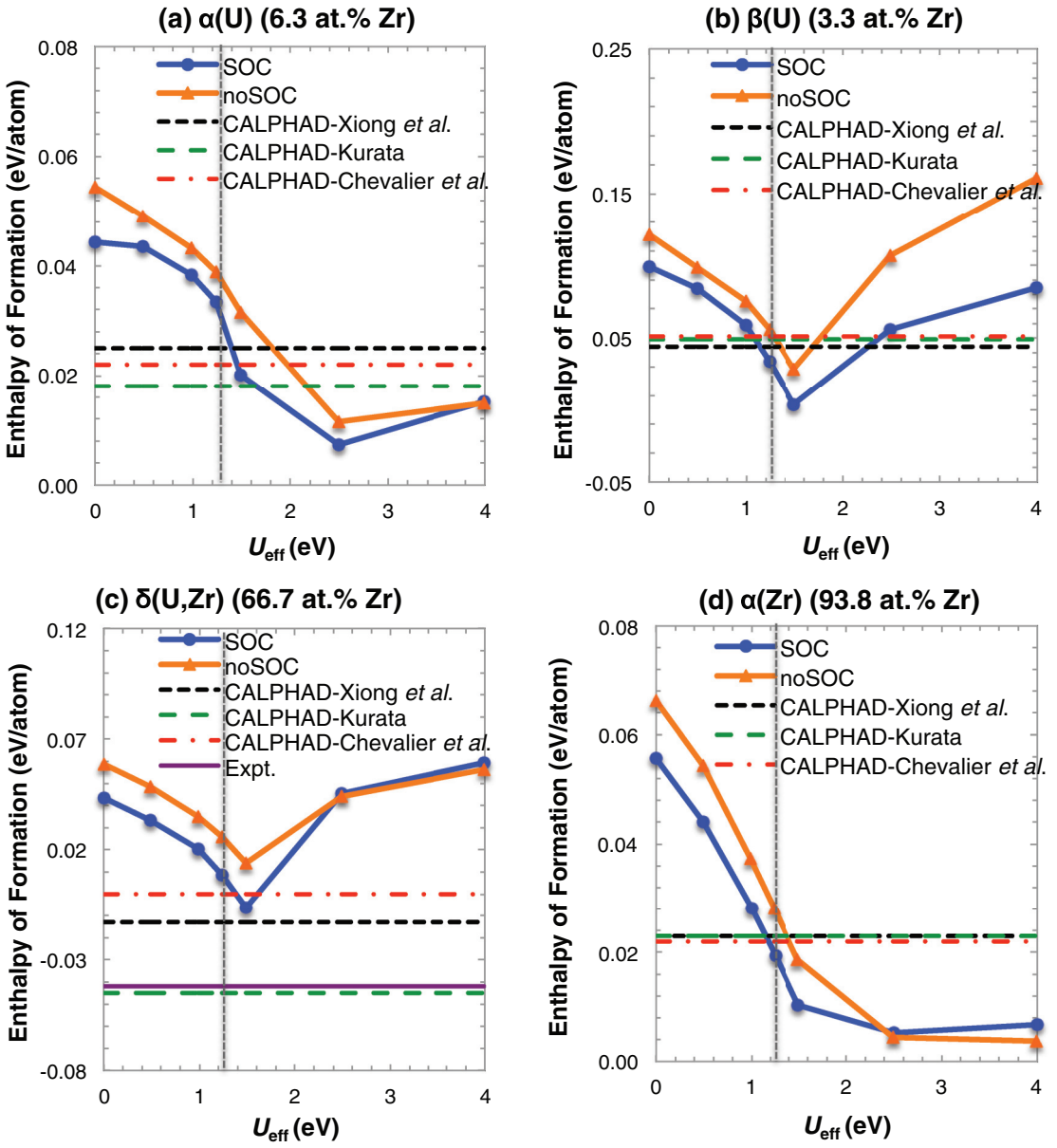

FIG. 3. (Color online) Enthalpy of formation for U-Zr alloy: (a) α(U) (6.3 at.% Zr), (b) β(U) (3.3 at.% Zr), (c) δ(U,Zr) (66.7 at.% Zr), and (d) α(Zr) (93.8 at.% Zr). The vertical dashed reference line is at $U_{\text{eff}} = 1.24$ eV. Experimental enthalpy of formation for δ(U,Zr), -0.04 ± 0.11 eV/atom, is from Nagarajan *et al.*;[78] the very large error bar is not plotted in panel (c). CALPHAD models are from Xiong *et al.*,[74] Kurata,[75] and Chevalier *et al.*[76]

reasonably well. As an example, we compare our calculated enthalpy of formation for γU in Table II. Our PAW calculation gives 0.241 eV/atom, which is very close to 0.223 eV/atom for FPLMTO,[16] 0.265 eV/atom for full-potential linearized augmented plane wave (FPLAPW),[13] and 0.249 eV/atom for linear combination of Gaussian-type orbitals–fitting function (LCGTO-FF)[13] and is essentially the same as that of another PAW study[19] (0.24 eV/atom, not tabulated in Table II). Besides U metal, our PAW calculations reproduce the mixing enthalpy of γ(U,Zr) from the EMTO and FPLMTO calculations of Landa *et al.*[27] as already mentioned above. What about EMTO? Interestingly, the same group of authors, Bajaj and Landa *et al.* in another study,[83] found a similarly large difference between their calculations using EMTO and FPLMTO for δ(U,Ti) that has the same C32 crystal structure as δ(U,Zr). For δ(U,Ti), their EMTO calculations gave a formation enthalpy of -0.402 eV/atom (-38.806 kJ/mol) while their FPLMTO gave -0.268 eV/atom (-25.865 kJ/mol)—the difference is -0.134 eV/atom (12.941 kJ/mol). Besides, they also estimated PAW would give -0.368 eV/atom (-35.483 kJ/mol) based on a third-party calculation,[84] which is also 0.034 eV/atom (3.323 kJ/mol) higher than EMTO's. Because δ(U,Ti) is completely ordered on both A and B sites, SQS or CPA is not necessary to model it, so it is clear that the difference should be between the EMTO and FPLMTO/PAW methods themselves. Considering EMTO gives a significantly lower enthalpy than FPLMTO for δ(U,Ti) and that FPLMTO is one of the most accurate full-potential methods, it is possible

TABLE II. Energetics[a] for solid phases of U, Zr metal, and U-Zr alloy.

		DFT (eV/atom)		DFT + U[b]		CALPHAD (eV/atom) (300 K)				
	Composition	(0 K)		(eV/atom) (0 K)		Xiong *et al.*	Kurata	Chevalier *et al.*	DFT refs.	Expt.
Phase	(at.% Zr)	noSOC	SOC	noSOC	SOC	(Ref. 74)	(Ref. 75)	(Ref. 76)	(eV/atom) (0 K)	(eV/atom) (var. T)
αU	0	6.375	6.246	5.421	5.326					5.55[g]
α(U)	6.3	0.058	0.044	0.046	0.041	0.025	0.018	0.022		
βU	0	0.110	0.063	0.086	0.049	0.033	0.033	0.033		
β(U)	3.3	0.125	0.099	0.078	0.062	0.044	0.049	0.051		
γU	0	0.282	0.239	0.205	0.173	0.099	0.099	0.099	0.223/ 0.265/ 0.249[c]	
	6.3	0.038	0.040	0.018 (0.023)	0.006 (0.021)	0.026	0.038	0.036		
	25.0	0.107	0.098	0.037 (0.058)	0.006 (0.036)	0.067	0.119	0.112	0.102[d]	
γ(U,Zr)	50.0	0.124	0.101	0.036 (0.058)	−0.006 (0.024)	0.060	0.150	0.138	0.120[d]	
	75.0	0.071	0.050	0.013 (0.027)	−0.012 (0.003)	0.026	0.107	0.097	0.067[d]	
	93.8	0.019	0.011	0.001 (0.006)	−0.007 (−0.003)	0.004	0.031	0.030		
βZr	100	0.079	0.078			0.076	0.076	0.076		
δ(U,Zr)	66.7	0.058	0.043	0.026 (0.014)	0.009 (−0.006)	−0.013	−0.045	0.000	−0.065[e]	−0.04 ± 0.1[h]
ωZr	100	0.001	0.001			0.005	0.011	0.000	0.006[f]	
α(Zr)	93.8	0.067	0.056	0.042	0.044	0.023	0.023	0.022		
αZr	100	6.160	6.158							6.25[g]

[a]Cohesive energy for αU/αZr, enthalpy of mixing for γ(U,Zr), and enthalpy of formation for all other phases.
[b]Result at $U_{\text{eff}} = 1.24$ eV is given for all; additional results at $U_{\text{eff}} = 0.99$ eV for γ(U,Zr) and at $U_{\text{eff}} = 1.49$ eV for δ(U,Zr) are also given in parentheses. DFT + U is not applied on Zr in all calculations.
[c]Soderlind's FPLMTO in Ref. 16, and Boettger's FPLAPW and LCGTO-FF in Ref. 13.
[d]FPLMTO-SQS result of Landa *et al.* in Ref. 27; their KKR-ASA-CPA result is similar and not tabulated but plotted in Fig. 5.
[e]EMTO-CPA results of Landa *et al.* in Ref. 27.
[f]Estimated from the FPLMTO result of Landa *et al.* (Fig. 9 in Ref. 27).
[g]Kittel in Ref. 72.
[h]Experimental result at 298 K from Nagarajan *et al.* in Ref. 78.

that EMTO similarly underestimates enthalpy for δ(U,Zr), hence explaining the large difference between our results and those of Landa *et al.*[27] using DFT.

What about DFT + U? Figures 2 and 3 show that when we apply DFT + U with a gradually increased U_{eff}, calculated energetics will first decrease and approach CALPHAD values. For example, DFT + U gives 0.009 and −0.006 eV/atom at $U_{\text{eff}} = 1.24$ and 1.49 eV, respectively, for the enthalpy of formation of δ(U,Zr), which are finally reasonable compared to both experimental and CALPHAD models. *Ab initio* energy curves generally cross the CALPHAD lines in the range between $U_{\text{eff}} = 1$ and 1.5 eV. The point of crossing varies somewhat among different systems and is usually before the point where the energy drops to a minimum near $U_{\text{eff}} = 2$ eV. After the minimal points, the curves rise drastically, and for most systems, they will cross the CALPHAD lines again. We stress that neither the minimal nor the second cross should be picked as the empirical U_{eff}, and we will explain the reason when we discuss the electronic structure below. Finally SOC and noSOC energetic curves in Figs. 2 and 3 show very similar qualitative features as functions of U_{eff}, but those of SOC are almost always below noSOC in the whole 0–4 eV range, showing that the inclusion of SOC will improve the energetics, which reflects correct physics and is expected for these actinide systems.

Putting all these energetic data together, let us look at the root mean square (RMS) of the differences between *ab initio* and CALPHAD energetics as a function of U_{eff} in Fig. 4. It shows that no matter which CALPHAD model we use for comparison, DFT always overestimates enthalpies significantly, and DFT + U always matches CALPHAD values better than DFT at $U_{\text{eff}} \sim$ 1–1.5 eV. A statistically optimal U_{eff} is 1.24 eV, although the RMS of differences is very close in the whole 1–1.5 eV range. Note we do not include the cohesive energy for αU in Fig. 4. The reason is that cohesive energy does not directly impact phase stability as modeled in CALPHAD, and including it will sweep the statistics because it is an order of magnitude larger than the formation enthalpies that are our major

TABLE III. Differences in enthalpy between DFT, DFT + U (1.24 eV), and CALPHAD for all solid phases of U metal and U-Zr except αU and γ(U,Zr).[a]

CALPHAD Model	Statistics of differences[b]	DFT (eV/atom)		DFT + U (eV/atom)	
		noSOC	SOC	noSOC	SOC
Xiong *et al*. (Ref. 74)	RMS	0.095	0.071	0.038	0.022
	Mean	0.081	0.060	0.027	0.009
	Max positive	0.183	0.140	0.079	0.045
	Max negative[c]	N/A	N/A	N/A	−0.010
Kurata (Ref. 75)	RMS	0.099	0.076	0.045	0.030
	Mean	0.086	0.065	0.032	0.014
	Max positive	0.183	0.140	0.079	0.053
	Max negative[c]	N/A	N/A	N/A	−0.015
Chevalier *et al*. (Ref. 76)	RMS	0.092	0.069	0.035	0.021
	Mean	0.077	0.057	0.024	0.006
	Max positive	0.183	0.140	0.079	0.045
	Max negative[c]	N/A[c]	N/A[c]	N/A[c]	−0.017

[a]αU is used as reference and γ(U,Zr) is controversial due to mechanical instability.
[b]Positive/negative difference means *ab initio* enthalpy is larger/smaller than CALPHAD enthalpy.
[c]N/A means none of the *ab initio* values is smaller than CALPHAD values.

interest. However, the trend in cohesive energy as a function of U_{eff} is similar to those found for the enthalpies in Figs. 2 and 3.

The above visual impressions from Fig. 4 are confirmed by quantitative statistics listed in Table III. The RMS of the differences in enthalpies between DFT and CALPHAD is approximately 0.10 and 0.07 eV/atom without and with SOC included, respectively. DFT + U at $U_{\text{eff}} = 1.24$ eV reduces it to 0.04 and 0.02 eV/atom. These together show that the improvement of DFT + U over DFT is ∼0.05 eV/atom (∼5 kJ/mol), and the effect of SOC is ∼0.02 eV/atom (∼2 kJ/mol). The former is a substantial amount of energy in the context of CALPHAD modeling, and the letter is relatively small. Our systematic model validation here shows that DFT significantly overestimates energetics, so it is beneficial to go beyond DFT to treat correlation in U and U-Zr for applications that requires high energetic accuracy, and DFT + U with $U_{\text{eff}} = 1.24$ eV seems a promising option. The relativistic effect of SOC is relatively small and may be included for applications that demand best accuracy.

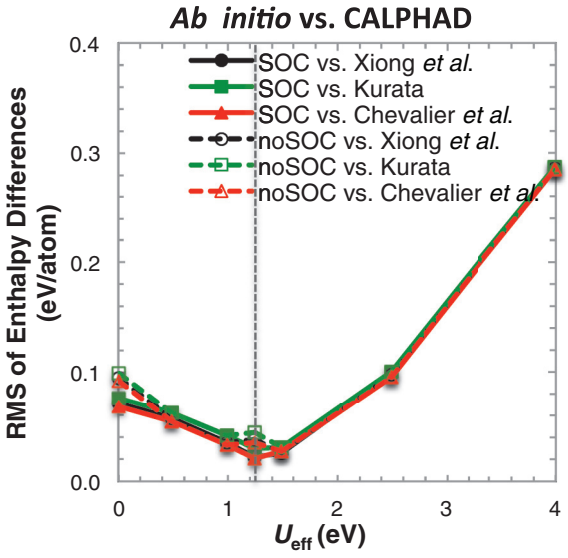

FIG. 4. (Color online) The RMS of enthalpy differences between *ab initio* and CALPHAD for all solid phases of U metal and U-Zr alloy except αU and γ(U,Zr). DFT is at $U_{\text{eff}} = 0$ eV, while DFT + U is at $U_{\text{eff}} > 0$ eV. CALPHAD models are from Xiong *et al*.,[74] Kurata,[75] and Chevalier *et al*.[76] See Table III for quantitative statistics.

With experiences gained on the above well-established phases, we now proceed to the controversial high-temperature bcc solid solution phase, γ(U,Zr), and show its enthalpy of mixing in Fig. 5. First of all, our DFT calculations using PAW-SQS give a strongly positive enthalpy (>0.1 eV/atom) that is overall symmetric as a function of composition in the whole region from 0 to 100 at.% Zr. As mentioned above when discussing δ(U,Zr), it is almost identical to the DFT result from FPLMTO-SQS of Landa *et al*.[27] (Fig. 5, circles), which is also very close to their DFT result from KKRASA-CPA[27] (crosses). Note they do not include SOC in either of the calculations, and we should compare their results to ours in the left panel of Fig. 5. These DFT results also reproduce well the CALPHAD results of Kurata[75] (green dashed curve) and Chevalier *et al*.[76] (red dashed curve), all suggesting strong demixing of bcc U and Zr. However, the latest CALPHAD model[74] (black dashed curve) gives a mixing enthalpy that is (1) only slightly positive and (2) asymmetric with the U-rich higher end. Based on our experience on the other phases in Figs. 2 and 3, our most accurate predictions should be from DFT + U at $U_{\text{eff}} = 1$–1.5 eV, which very interestingly all also give weekly positive (or even slightly negative on the Zr-rich end) and asymmetric mixing enthalpy. It should be pointed out that this latest CALPHAD model by Xiong *et al*.[74] was developed in our group with knowledge of the *ab initio* results reported here; however, an attempt was deliberately made *not* to fit its model parameters to our *ab initio* results, but only to available experiments in order to provide an independent source of reference. Showing excellent match with experimental phase boundary and heat capacity data in

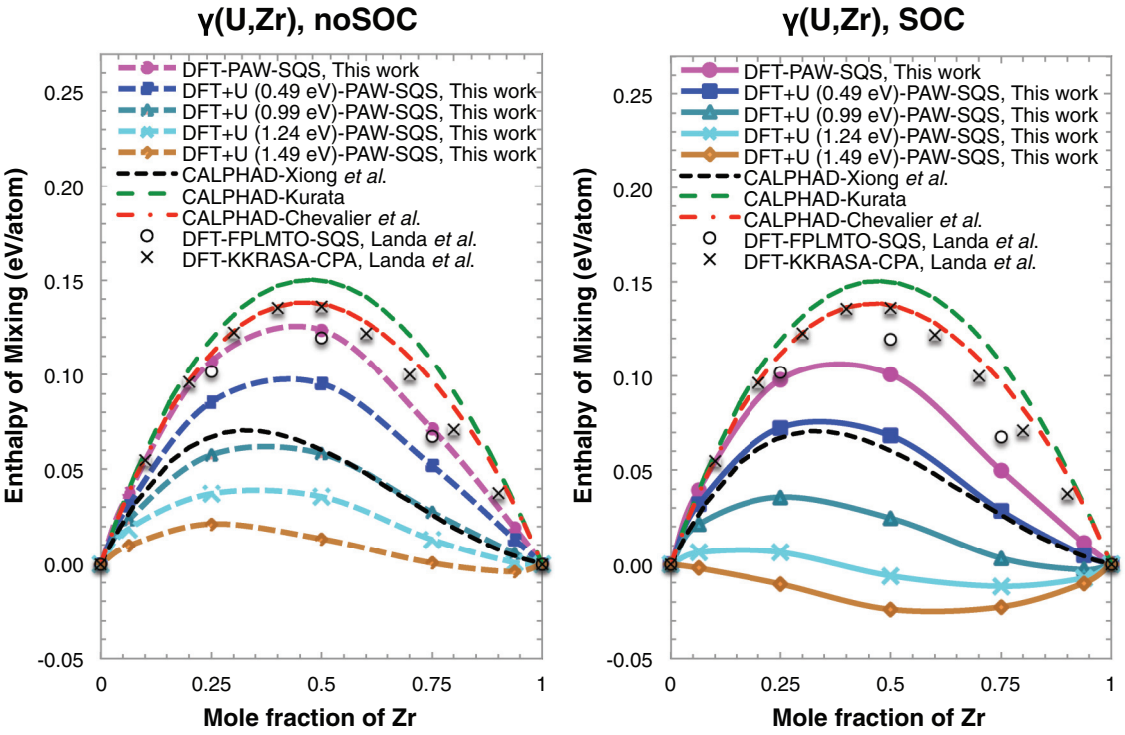

FIG. 5. (Color online) Enthalpy of mixing for γ(U,Zr). DFT results are from the noSOC calculations of Landa *et al*. (Ref. 27); CALPAHD models are from Xiong *et al*.,[74] Kurata,[75] and Chevalier *et al*.[76] U_{eff} used for DFT + U is given in parentheses in the legend.

wide composition and temperature ranges, the CALPHAD model of Xiong *et al*.[74] is in no way less accurate and in some ways more accurate than previous CALPHAD models, suggesting that the weaker demixing found here is possible and does not contradict existing experimental data. Note that our DFT + U result at 1.24 eV from SOC is slightly negative on the Zr-rich end and is about 0.04 eV/atom below at the maximum point from that of Xiong *et al*., while the one at $U_{\text{eff}} = 0.99$ eV or even 0.49 agrees with it better. It is possible that we should use a smaller U_{eff} value, for example 1 eV for γ(U,Zr), rather than 1.24 eV, because as we see in Figs. 2 and 3, the point of U_{eff} where DFT + U curves cross CALPHAD varies slightly between 1 and 1.5 eV among different phases. However, due to the possible error in our *ab initio* energetics resulting from constrained relaxation and other approximations, and considering the error bar of CAPHAD energetics, the two sets of energetics can still be considered reasonably consistent. Besides all the above modeling studies, one experimental measurement of the mixing enthalpy of γ(U,Zr) by electromotive force (emf) at 1073 K (Ref. 79) is available (not plotted in Fig. 5). The emf result is substantially negative, explaining the complete miscibility between bcc U and Zr at such high temperature. Due to the huge temperature difference, our modeling results cannot be directly compared to it in terms of quantitative values. Yet it is interesting to note that the emf enthalpy is also *asymmetric* with U-rich higher end. The fact that both our DFT + U calculation and the latest CALPHAD model[74] reproduce the same asymmetry of the experimental emf data suggests that our prediction is possibly closer to the true value. Overall, there are still controversies on this high-temperature phase due to the scattering of previous results, the scarcity of direct experimental thermochemical data, and the uncertainty resulting from our model approximations, and we call for more experimental measurements to resolve this controversy.

Next we present the calculated volume, which is tabulated in Table IV for all systems of U, Zr metal, and U-Zr alloys at the two U_{eff} points of 0 and 1.24 eV only, as well as plotted in Fig. 6 for U metal and U-Zr alloy only in the whole region of $U_{\text{eff}} = 0$–4 eV. Again, we discuss the results in terms of DFT vs DFT + U, and noSOC vs SOC.

First, for the three phases of U metal, volumes calculated by DFT are smaller than the experimental data. The point is best illustrated by αU, as it is the stable phase of U metal at 0 K (the ground state phase) that has direct low-temperature experimental data[44] available. As tabulated in Table IV, the experiment in Ref. 44 measured its volume to be 20.53 Å^3/atom at 45 K (just above charge density wave states at 43 K and below), which is corrected to be 20.48 Å^3/atom at 0 K with Debye-Gruneisen quasiharmonic model.[85] Using PAW, we get 20.06 and 20.07 Å^3/atom from noSOC and SOC calculations, respectively, which are about 2% smaller than experimental values. They are quite close to what was obtained in a previous PAW study:[19] 20.19 and 20.07 Å^3/atom from noSOC and SOC calculations, respectively (not tabulated in Table IV). To see if the error is due to the pseudopotential approximation of PAW, we further compare them to *ab initio* results obtained from full-potential methods. The FPLMTO method[16] obtained ~20.40 (estimated from Fig. 6 in Ref. 16) and 20.67 Å^3/atom from noSOC and SOC calculations, respectively. However, an earlier SOC calculation[10] using the same FPLMTO method and GGA functional obtained 19.49 Å^3/atom (not tabulated in Table IV). Another full-potential method, FPLAPW,[13,14] gives 20.41 and 20.76 Å^3/atom from noSOC and SOC calculations,

TABLE IV. Volume for solid phases of U, Zr metal, and U-Zr alloy (Å^3/atom).

Phase	Composition (at.% Zr)	DFT (0 K) noSOC	DFT (0 K) SOC	DFT + U (1.24 eV) (0 K) noSOC	DFT + U (1.24 eV) (0 K) SOC	DFT refs.	Expt. (var. T)	Expt. (Corrected to 0 K)[f]
αU	0	20.06	20.07	20.75	20.94	20.40/20.67; 20.41/20.76; 20.34 (0 K)[a]	20.53 (45 K) (Ref. 44)	20.48
α(U)	6.3	20.50	20.57	21.19	21.39			
βU	0	20.49	20.49	21.51	21.91		21.81 (955 K) (Ref. 45)	21.19
β(U)	3.3	20.63	20.62	21.75	22.07			
γU	0	20.13	20.17	21.28	22.77	20.43/20.74; 20.51 (0 K)[b]	22.05 (1060 K) (Ref. 45)	21.46
γ(U,Zr)	6.3	20.36	20.41	21.96	22.79			
	25.0	21.10	21.18	22.62	23.20	22.25 (300 K)[c]	22.37 (room T) (Ref. 50)	22.15
	50.0	21.97	22.06	23.02	23.33	22.90 (300 K)[c]	22.29 (room T) (Ref. 50)	22.07
	75.0	22.43	22.60	23.04	23.23	23.52 (300 K)[c]	22.75 (room T) (Ref. 50)	22.63
	93.8	22.88	22.86	23.01	22.97			
βZr	100	22.91	22.91			22.98 (0 K)[d]	23.70 (1253 K) (Ref. 49)	23.10
δ(U,Zr)	66.7	22.61	22.68	22.99	23.17	22.49 (0 K)[e]	22.49 (room T) (Ref. 51)	22.36
ωZr	100	23.28	23.31			23.14 (0 K)[d]	22.75 (room T) (Ref. 48)	22.65
α(Zr)	93.8	23.54	23.55	23.66	23.68			
αZr	100	23.52	23.55			23.43 (0 K)[d]	23.22 (4.2 K) (Ref. 47)	23.19

[a]Soderlind's FPLMTO noSOC/SOC results in Ref. 16 (noSOC estimated from Fig. 6); Jones *et al.*'s FPLAPW noSOC/SOC results in Ref. 14; and FPLMTO SOC result from Le Bihan *et al.* in Ref. 86 (noSOC not given).
[b]Soderlind's FPLMTO noSOC/SOC results in Ref. 16 (both estimated from Fig. 6); Boettger's FPLAPW noSOC result in Ref. 13 (SOC not given).
[c]Landa *et al.*'s KKRASA-CPA noSOC results at 300 K in Ref. 27 (estimated from Fig. 1).
[d]Landa *et al.*'s FPLMTO noSOC results at 0 K in Ref. 27.
[e]Landa *et al.*'s EMTO-CPA noSOC results at 0 K in Ref. 27.
[f]Based on Debye-Gruneisen quasiharmonic model in Ref. 85 (see Supplemental Material[87]).

respectively. The full-potential values are about 2% larger than our PAW values, so the pseudopotential approximation probably has contributed part of the underestimation. However, there is another subtle difference that may play an even more important role. αU has an internal parameter (often denoted y) that determines the atom positions and early full potential calculations usually either set y to experimental value and do not relax the atom positions when relaxing the lattice constants, or as Ref. 16 did, manually perform loops of sequential relaxation of lattice constants and y parameter that stop when certain convergence criteria is met. In contrast, our pseudopotential PAW calculations fully relaxed the lattice constants and atom positions simultaneously with conjugate-gradient (CG) algorithm. Interestingly, a more recent full potential SOC calculation with FPLMTO[86] that also did simultaneous relaxation of all structural degrees of freedom of αU with CG algorithm obtained a value of 20.34 Å^3/atom, which is over 1.5% smaller than the full potential results in Refs. 14 and 16 and much closer to our PAW value. Reference 86 did not report any result from noSOC calculation but the effect of relaxation should be similar. In short, full-potential values, at least from noSOC calculations, are smaller than the experimental value by about 1% and perhaps more if the structure is also properly relaxed with CG algorithm; those from SOC calculations are not all consistent.the smallest value is 5% below, the largest is about 0.5% over, and the latest and perhaps most accurate value in Ref. 86 is about 0.7% below the experimental value. This is unusual because DFT calculations based on GGA more often overestimate volume. For example, in a previous high-throughput study[89] of 10 768 compounds in the International Crystal Structure Database, it is found that the median error for DFT-GGA's volume prediction is positive (i.e., overestimated) 3.2%; also as a specific example, as listed in Table IV, our own calculations show that DFT-GGA overestimates the volume of αZr by about 1.3%. So, if it is still debatable to suggest that DFT-GGA underestimates the volume of U metal in the absolute sense, it is reasonable to argue that at least DFT-GGA's volume prediction for U metal is biased toward the negative (i.e., underestimated) end in the statistical distribution of the volume prediction errors. Such a finding is not surprising. In fact, it follows the general trend of DFT-GGA's underestimation of the volume of actinide metals.[14] The trend debatably starts at U, as we have discussed above, and becomes more significant as the atomic number increases—for Np and Pu, the calculated volumes are clearly smaller than experimental values, even in the most

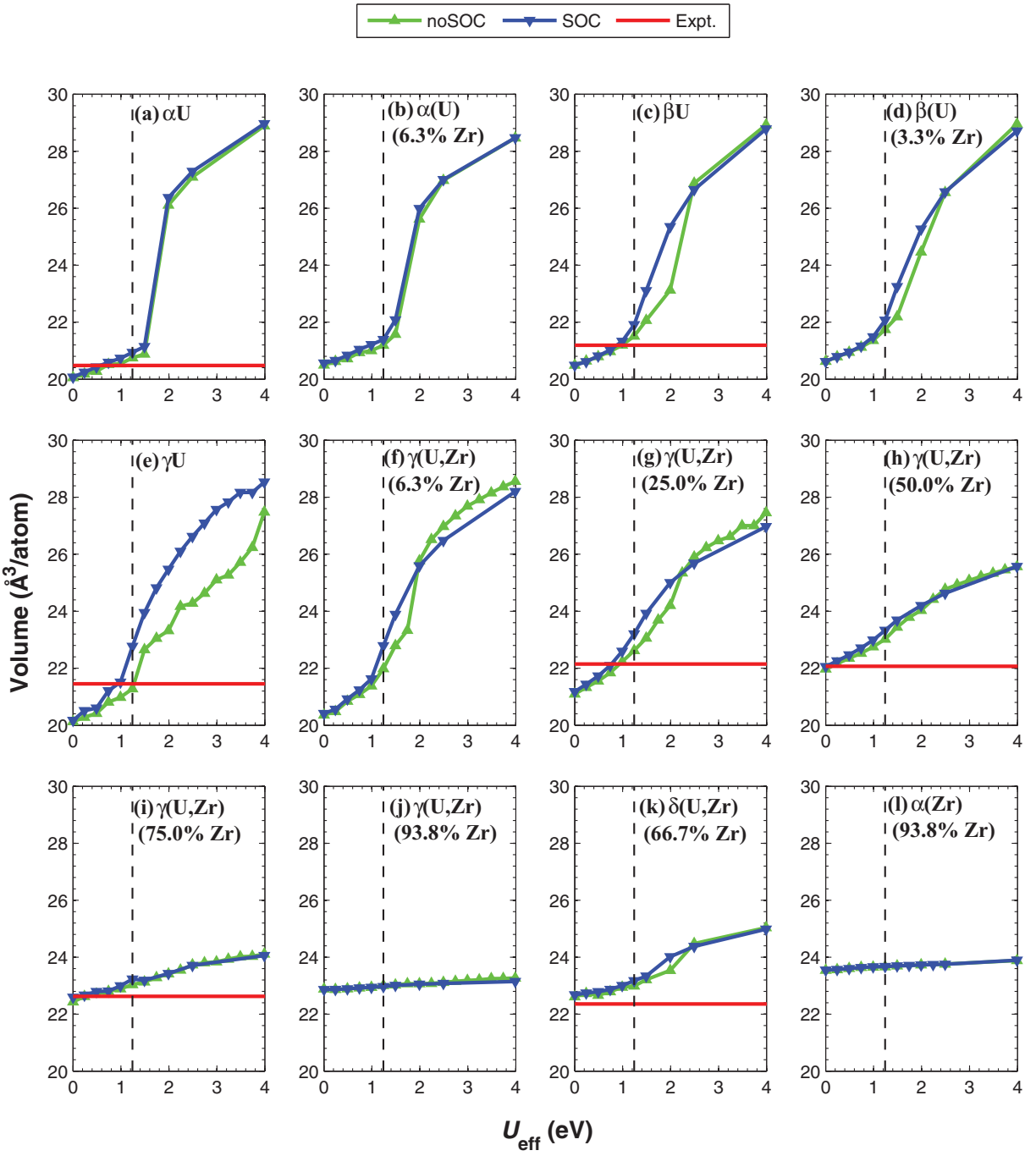

FIG. 6. (Color online) Volume for all solid phases of U metal and U-Zr alloy as a function of U_{eff}: (a) αU; (b) α(U) (6.3 at.% Zr); (c) βU; (d) β(U) (3.3 at.% Zr); (e) γU; (f) γ(U,Zr) (6.3 at.% Zr); (g) γ(U,Zr) (25.0 at.% Zr); (h) γ(U,Zr) (50.0 at.% Zr); (i) γ(U,Zr) (75.0 at.% Zr); (j) γ(U,Zr) (93.8 at.% Zr); (k) δ(U,Zr) (66.7 at.% Zr); and (l) αZr (93.8 at.% Zr). The vertical dashed reference line is at $U_{\text{eff}} = 1.24$ eV. Experimental data are from those referenced in Table IV corrected to 0 K; no direct experimental data are found for panels (b), (d), (f), (j), and (k).

accurate full-potential calculations with SOC included (see Table I of Ref. 14). Since the correlation effects become more pronounced with higher atomic number along the actinide series, it is expected that the volume underestimation is due to correlation effects.

Next we discuss Zr metal. Table IV shows that our PAW results for Zr metal match the full potential results from FPLMTO[27] very well for all the three solid phases of Zr. In comparison, we note that our earlier calculations using a different PAW pseudopotential for Zr that only treated $5s^2 4d^2 5p^0$ as valence orbital obtained considerably smaller volumes, which prompted us to adopt the current pseudopotential for Zr. Comparing to experimental data, our current DFT-GGA calculations overestimate the volume of αZr and ωZr by about 1.3% and 2.6%, respectively, while marginally underestimate the volume of βZr (<0.8%).

Now we discuss U-Zr alloy. We have found experimental volume data for γ(U,Zr) at 25, 50, and 75 at.% Zr and for δ(U,Zr) at 66.7 at.% Zr. For γ(U,Zr), DFT also underestimates the volumes to different extents, and if we consider it together with γU metal, the error seems to decrease as Zr concentration increases and becomes negligible at 50 and 75 at.% Zr. The result is expected because γ(U,Zr)'s end members are βZr and γU (they all have bcc structure) and we have shown above that DFT almost reproduces the volume for βZr but underestimates that for γU significantly. δ(U,Zr)'s volume are 22.61 and 22.68 Å^3/atom from noSOC and SOC calculations, respectively, which, different from all other U and U-Zr phases are nevertheless larger than the experimental value[51] of 22.49 Å^3/atom at room T (22.36 if corrected to 0 K). This result seems to be an anomaly but is totally expected because the volume of ωZr, which is the end member of δ(U,Zr) that also has C32 structure, is overestimated by a significant extent of 2.6%—in contrast with βZr whose volume is even slightly underestimated. Our PAW results based on both Zr PAW potentials are again different from the EMTO result of Landa *et al.*,[27] which does not include SOC but matches the experimental value almost perfectly. The discrepancy can be due to reasons similar to those that explain the difference in our calculated enthalpies for δ(U,Zr) discussed above but can also stem from approximations in our calculations, such as the pseudopotential. Other alloyed phases do not have direct experimental volume data, but we can assume the trend will be similar.

Now we consider the effect of adding $+U$ potential on volume. Qualitatively, Fig. 6 shows that the calculated volumes increase monotonically with U_{eff} from 0 to 4 eV for all 12 systems. The evolution can be differentiated into three linear stages with the first having the smallest slope and the second the largest. The phenomenon is negligible at 93.8 at.% Zr for both γ(U,Zr) and α(Zr) but becomes more pronounced with increased U concentration and is most obvious in αU. We will keep finding such three-stage differentiation on other calculated properties below. Next we make quantitative comparison of calculated volume with experimental results that we find for seven systems, as listed in Table IV. Firstly, for U metal and U-rich U-Zr alloy (i.e., αU, βU, γU, and γ(U) at 25 at.% Zr), optimal match of calculated volume with experimental value seems to happen at U_{eff} around 1 eV. Secondly, for U-Zr alloy with higher Zr contents (i.e., γ(U,Zr) at 50 and 75 at.% Zr, and δ(U,Zr) at 66.7 at.% Zr), DFT already reproduces well or even overestimates the volume. Because DFT + U always gives larger volume than DFT, it obtains worse agreement with experimental data at almost any finite U_{eff}. Does this mean DFT + U is a worse model for Zr rich U-Zr alloy systems than DFT? The answer is certainly no. The reason is that for U-Zr alloy, DFT + U is only applied on the U sublattice, and any error on the Zr sublattice remains largely unchanged not matter what U_{eff} is used. The error on Zr sublattice carries negligible weight in the U rich system γ(U,Zr) at 25 at.% Zr discussed above, but becomes more important or even dominant when Zr content is larger. Take δ(U,Zr) at 66.7 at.% Zr as an example. DFT overestimates its volume by 1%. In comparison, DFT overestimates its end member ωZr's by 2.6%. The error for δ(U,Zr) is smaller than ωZr only because for δ(U,Zr) DFT's volume overestimation error on the Zr sublattice in δ(U,Zr) is partially canceled by the underestimation error on the U sublattice. Because Zr is dominant at 66.7 at.% Zr, the overall error is still positive (i.e., overestimation). When DFT + U is used, the error on the U sublattice is reduced and can cancel less the error on the Zr sublattice, which results in the net effect of increased overall error at larger U_{eff}. At $U_{\text{eff}} = 1$ eV, DFT + U gives volume of δ(U,Zr) that is overestimated by 2.9%, which is approximately the error for ωZr. This result suggests that the error on the U sublattice almost vanishes at 1 eV, which is in excellent agreement with the results for U metal and U-rich U-Zr alloy systems discussed above. Therefore, DFT + U is still more appropriate than DFT for δ(U,Zr). Similar argument holds for γ(U,Zr) although the trend is less clear due to noises in the data introduced by the various approximations mentioned above, especially the constrained relaxation. Overall, the above quantitative comparison shows that volume fitting gives an empirical optimal U_{eff} near 1 eV, with 1.24 eV being marginally worse. The situation for volume should be compared with that for enthalpy, for which Fig. 4 shows the optimal U_{eff} is near 1.24 and 1 eV is only slightly inferior. For both enthalpy and volume, the difference between those at 1 and 1.24 eV is comparable to the combined error bar of our *ab initio* calculation, the experimental data and the temperature extrapolation. Therefore, we can consider fittings in volume and enthalpies to give consistent empirical U_{eff}.

Regarding the effect of SOC on volume, for all systems in Fig. 6, volumes from SOC calculations are slightly larger than (<0.5%) or at least equal to those from noSOC when using both DFT and DFT + U, with U_{eff} in the reasonable range of 0–2 eV (the meaning of "reasonable" will become evident after we discuss other calculated properties below). This is especially true for all three solid phases of U metal, which reflect correct physics[88] and agree with previous full-potential studies using FPLMTO[16,88] and FPLAPW,[13,14] as we have discussed above.

On the whole, the above results of calculated volumes suggest that correlation effects also have a significant impact on volume: based on GGA, DFT underpredicts the volume of U metal and the U sublattice in U-Zr alloy, and the error is somewhat corrected using DFT + U. The relativistic effect of SOC is also relevant, which increases the volume and brings in further improvement. Such results on volume are consistent with those on energetics discussed above.

The calculated spin, orbital, and total magnetic moments integrated over the whole unit cell are given as functions of U_{eff} for all solid phases of U metal and U-Zr alloy in Fig. 7. The magnetic moments evolve in three stages as well. Initially, total magnetic moments are zero for all systems; spin/orbital moments are also zero for U metal and U-Zr alloy with high U concentrations and are finite but small for U-Zr alloy with low U concentration. After a threshold value of U_{eff}, total magnetic moments emerge and start to increase with larger U_{eff}. Finally, these moments level out after reaching a certain saturation level. The empirical optimal $U_{\text{eff}} = 1.24$ eV from energetic and volume fitting in general lies in the first stage. We comment on the magnetic configurations of U and U-Zr next. Experimentally, αU is confirmed Pauli paramagnetic with vanishing local magnetic moments (<0.005 μ_B/atom),[67,68] and βU and γU show

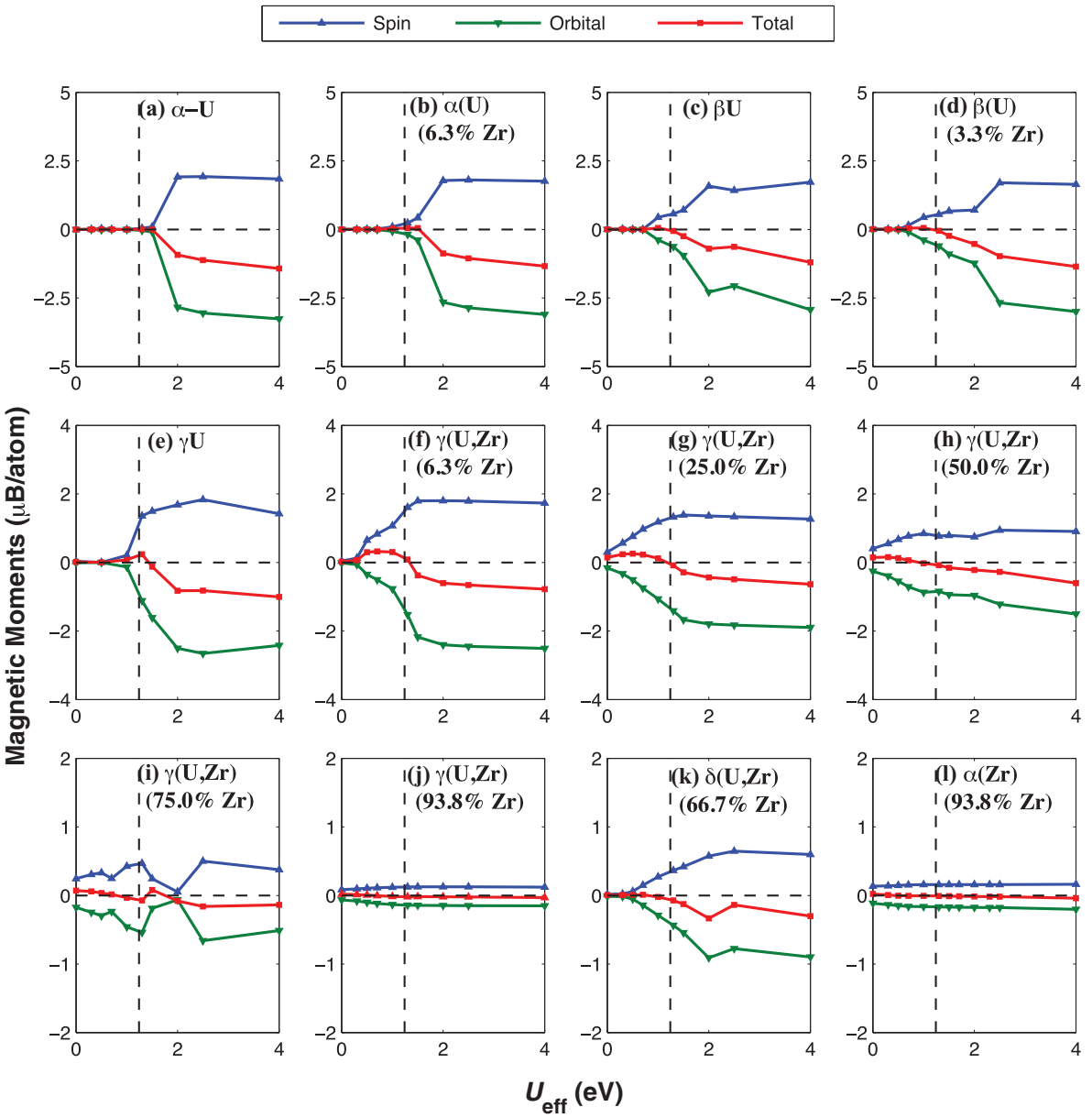

FIG. 7. (Color online) Integrated spin, orbital, and total magnetic moments for all solid phases of U metal and U-Zr alloy as functions of U_{eff}: (a) αU; (b) α(U) (6.3 at.% Zr); (c) βU; (d) β(U) (3.3 at.% Zr); (e) γU; (f) γ(U,Zr) (6.3 at.% Zr); (g) γ(U,Zr) (25.0 at.% Zr); (h) γ(U,Zr) (50.0 at.% Zr); (i) γ(U,Zr) (75.0 at.% Zr); (j) γ(U,Zr) (93.8 at.% Zr); (k) δ(U,Zr) (66.7 at.% Zr); and (l) αZr (93.8 at.% Zr). The vertical dashed reference line is at $U_{\text{eff}} = 1.24$ eV. Only results from SOC calculations are shown here and those from noSOC are similar. The directions of spin magnetic moments are taken to be positive. Orbital moments are in general antiparallel to spin moments and thus negative. The unsmooth segment between 1.5 and 2.0 eV for γ(U,Zr) (75.0 at.% Zr) might be metastable solutions; their spin and orbital moments are not collinear, so the signs of the total moments only indicate which of the two moments dominate.

similar behavior in magnetic susceptibility measurements.[90] Our DFT calculations indeed get zero magnetic moments on every atomic site for the three phases of U metal and therefore correctly reproduce its magnetic structure. For U-Zr alloy, DFT also gets no local magnetic moments on the U-rich end but does yield some spin and orbital moments on the Zr-rich side, which are on U rather than Zr atomic sites, though. Note that γ(U,Zr)'s results here are from constrained relaxation only. If fully relaxed, they are also found to have vanishing local spin and orbital magnetic moments, so the presence of these moments may be an artifact of the constrained relaxations we are using to treat this unstable phase. On the other hand, DFT + U at $U_{\text{eff}} = 1.24$ eV in general gets nonzero local *spin* magnetic moments for at least some of the atomic sites, even in U metal. However, these moments are close to zero for U metal and not exceeding 2 μ_{B} even in the Zr-rich U-Zr alloy systems; moreover, the local spin moments are also largely canceled by orbital moments. Take αU as an example. At $U_{\text{eff}} = 1.24$ eV the spin moments for αU on each of the two atomic sites are 0.045 μ_{B} and the orbital moments are -0.043 μ_{B}. The

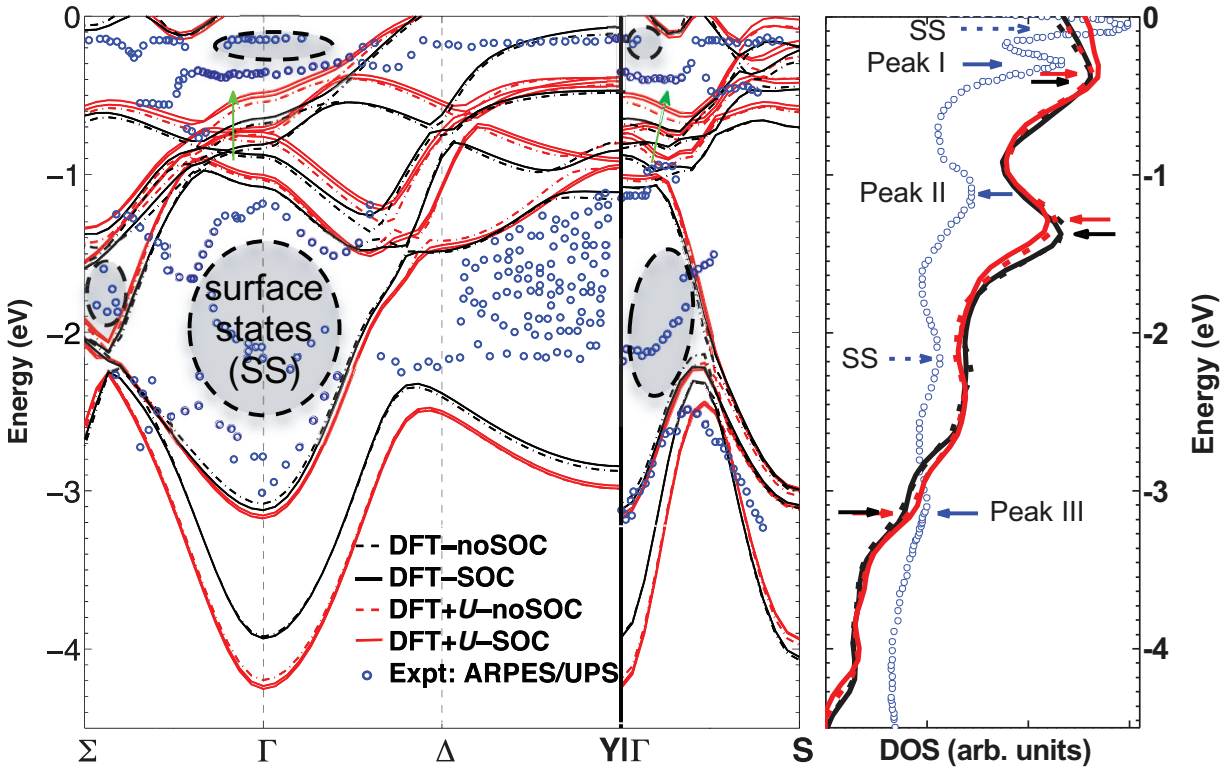

FIG. 8. (Color online) Band structure (left panel) and density of states (right panel) for αU. The respective experimental references are ARPES spectra from Opeil *et al.*[33] and UPS spectra from Opeil *et al.*[32] for the αU (001) single crystal. All experimental spectra are plotted as blue circles, while calculated results of DFT and DFT + U ($U_{\text{eff}} = 1.24$ eV) are plotted as black and red curves, respectively; solid and dashed lines distiguish noSOC and SOC, respectively. On the left, green arraws indicate two representative improvements of bands going from DFT to DFT + U. On the right, the positions of peaks from experimental, DFT, and DFT + U are marked with blue, black, and red arrows, respectively. Gray areas on the left and dashed arrows on the right indicate spectrum features from surface states that are not modeled in the calculations. Only the occupied part between −4.5 and 0 eV relative to the Fermi level is shown. See Fig. 2 in Ref. 33 for an illutration of the Brillouin zone and the special k points used here.

uncompensated 0.002 μ_B total local moments are antiparallel between the two sites and give zero integrated total magnetic moments. For other systems with larger supercells, local magnetic moments, if existing, are quite random in terms of both magnitude and direction, and we do not observe any long-range ferromagnetic or antiferromagnetic ordering. Most importantly, the total magnetic moments on each atomic site are still zero or very small at $U_{\text{eff}} = 1.24$ eV. Therefore, DFT + U at $U_{\text{eff}} = 1.24$ eV still gives no ordered magnetism for U and U-Zr. In short, DFT + U promotes spin/orbital polarization, which is still quenched at small U_{eff} but emerges at larger U_{eff}. At the empirical 1.24 eV, total local magnetic moments are still zero or vanishingly small in general, which is consistent with experiments showing no local moments. However, our results do show significant local spin and orbital moments in some cases, although they almost completely cancel each other. These values are difficult to compare to experiment and we cannot be sure if they might exist in nature—it is quite possible that they are an artifact of the current DFT + U functional because the Hartree-Fock term in it is well known to promote magnetic polarization. This artifact can probably be avoided by employing an alternative double counting scheme so called around the mean field (AMF), as Ref. 91 showed that AMF gives magnetic polarization a much larger penalty than FLL double counting scheme that we are using in this study. In fact, AMF based DFT + U has been validated on δPu in Ref. 92 to yield a nonmagnetic ground state in perfect agreement with experiment result while still reproduce the experimental volume, bulk modulus and important features of photoelectron spectra well and significantly better than DFT. We will leave it for future study to consider AMF based DFT + U for U and U-Zr. At present, we conclude the discussion by pointing out that it would be misguided to be overly concerned with the emergence of very small moments in isolated incidents when the energetics, volume and electronic structure (discussed next) are globally improved.

Next we show that DFT + U's improvement in the calculated energy and volume relative to DFT is not fortuitous—it is based on a better account of the electronic structure. We make the case on the experimentally most characterized system αU by comparing its calculated valence band electronic structure to experimental photoelectron spectra in Figs. 8 and 9.

We first focus in Fig. 8 on the occupied part between −4.5 and 0 eV relative to the Fermi level. Here, the latest experimental angle-resolved photoemission spectroscopy (ARPES)[33] and ultraviolet photoemission spectroscopy (UPS)[32] spectra of the αU (001) single crystal are used as references for the

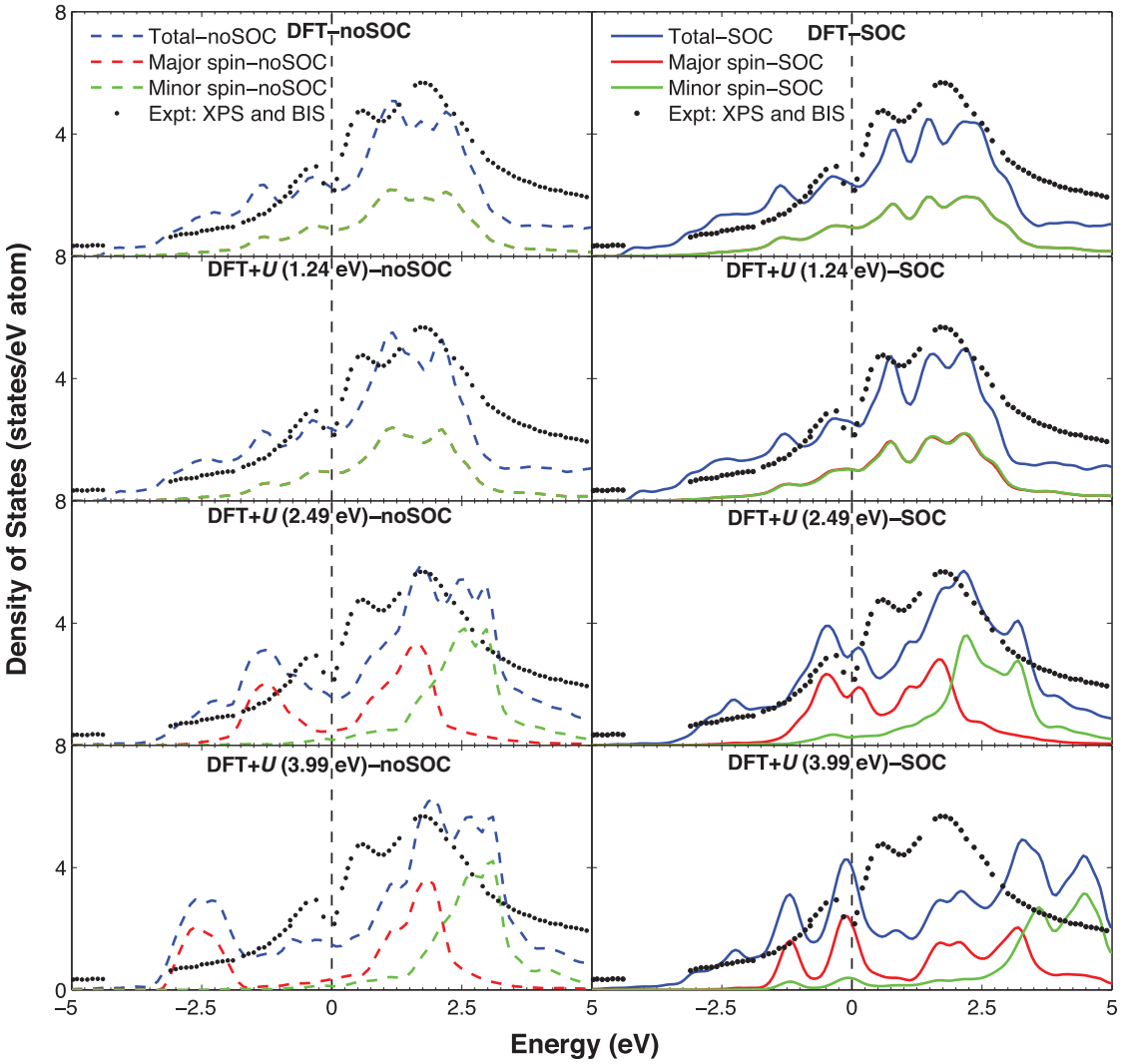

FIG. 9. (Color online) Density of states for αU as a function of U_{eff}. The vertical dashed reference line is Fermi level. Experimental reference is the XPS and BIS spectra of Baer and Lang.[93] The full valence band, both occupied and unoccupied, is shown.

calculated band structure (left panel) and DOS (right panel) of bulk αU, respectively. Before we start the comparison, a few clarifications regarding the experimental spectra should be made. First, some features of the spectra are due to surface states as the escape depth of the phonon source used is "at most 2–3 atomic layers."[33] Some of the possible surface states features are suggested based on DFT calculations of bulk αU.[32,33] These features are marked roughly with gray areas in the left and dashed arrows in the right panel of Fig. 8. They are not expected to exist in our *ab initio* results. Second, the UPS spectra in Fig. 8 reflect states mainly along the ΓZ direction (we follow the k-point designation given in Fig. 2 of Ref. 33). Our calculated DOS is however total DOS (TDOS) integrated over the whole Brillouin zone and thus may show additional features not seen in the UPS spectra. On the other hand, the ARPES spectra reflect mainly states along k-vectors in the (001) plane that is normal to ΓZ, so the ARPES and UPS spectra may not strictly align with each other. However, the anisotropy of electronic states for such a metallic system should be small, and we can probably still make meaningful comparisons between the three groups of data. Finally, the UPS spectra are not normalized, so their absolute intensity is not comparable to the calculated DOS, and we should focus the comparison on energy.

Now we start our discussion with the right panel of Fig. 8. There, the UPS spectra mainly show five peaks at -0.1, -0.3, -1.2, -2.2, and -3.2 eV, respectively, which are marked with blue arrows. The two at -0.1 and -2.2 eV are suggested to be surface states,[32] and their arrows are dashed and annotated with text. The remaining three peaks all show up in the calculated TDOS, which are marked correspondingly with black and red arrows for DFT and DFT $+ U$. Moreover, two additional small peaks also exist near -2.7 and -4.2 eV (not marked) in the calculated TDOS, which are not seen in the UPS spectra (not to confuse the TDOS peak near -2.7 eV with the UPS surface state peak near -2.2 eV). As explained above, they are presumably from electronic states along other directions of the Brillouin zone, for example, those shown in the left panel of Fig. 8. In fact, the positions of these additional two DOS peaks are consistent with where some bands turn around on the left. We neglect the two UPS peaks due to surface states and the two TDOS peaks not existent along the ΓZ direction and focus on

the three peaks near −0.3, −1.2, and −3.2 eV. For the sake of convenience, we will refer to them as peak I, peak II, and peak III, respectively, henceforth. Figure 8 shows that peak I and peak II from DFT shift downward to −0.4 eV and −1.4 eV, respectively, while peak III does not change much relative to UPS. To see if the difference is due to the direction of the UPS spectra, we cite the directional DOS calculated exactly along ΓZ with DFT-GGA in Ref. 32, which shows that peak I also downshifts to −0.6 eV, while peak II and III are rather well reproduced. So the error of downward shifting of peak I should be real while that of peak II is possibly artificial and due to anisotropy. Such a result is expected. If we look at the orbital projected DOS of αU in the first row of Fig. 10, we will find that f states dominate, mainly above −1.3 eV. So peak I is mainly due to f states, while peak II and III are probably more of other states (e.g., s and d states). The above analysis points to peak I as a key indicator of the correlation effects and how well they are modeled. Now we present a key point of Fig. 8: peak I from DFT + U is shifted upward with respect to DFT to around −0.35 eV, partially correcting the downward shifting error and is therefore in better agreement with UPS. The shift in energy seems relatively small (about 0.1 eV), but peak I is directly below Fermi level and has the largest magnitude among the peaks below Fermi level, so the effect is still significant. Besides position, the magnitude of peak I from DFT + U is also larger than DFT. It is in fact another improvement that is not evident in Fig. 8, in which the UPS spectra's absolute magnitude is not meaningful, as mentioned above, but will become clear below when compared to the properly normalized spectra in Fig. 9. All these factors make the seemingly small change in peak I a substantial improvement.

Next we show that we can draw similar conclusions from band structure, which is shown along the three k-vectors Σ-Γ, Γ-Δ-Υ, and Γ-S in the left panel of Fig. 8. In general, six bands exist between −0.2 and −4.5 eV in all the three directions, although the highest of them actually extends above Fermi level between Δ-Υ. We will name them bands I, II, . . ., and VI from top to bottom, respectively. They can be easily identified near Γ, although bands II and III are almost degenerate at Γ. The band that is directly above the six also has some segments extending below Fermi level to about −0.2 eV, which shows up in the Σ-Γ and Γ-S directions, but its major parts are above it and unoccupied, and thus we will neglect it in our discussion below. For the band structure calculated by DFT (black curves), our result is generally consistent with the DFT calculation of Opeil *et al.*[33] (not shown in Fig. 8), but two major differences exist, which may be due to factors like the pseudopotential approximation used in our calculation and the lack of structural relaxation in theirs.[33] The first difference is that band V and band VI are almost degenerate at Γ in Ref. 33 but are about 0.8 eV split in Fig. 8. Nevertheless, bands V and VI are low lying and mostly not f states, so they are expected not to affect the property of U metal much. The other difference happens on all five bands II–VI along Δ-Υ (remember band I is above Fermi level there). For example, Ref. 33 has band II also above Fermi level, like band I, while our calculation shows band II to be between −0.1 and −0.8 eV. Despite this, it should be noticed that Δ and Υ are relatively low symmetry k points and carry much less weight compared to high-symmetry k points such as Γ. Encouragingly, our calculations show good agreement with those of Opeil *et al.*[33] for bands I–IV around Γ (i.e., Σ-Γ, Γ-Δ, and Γ-S), which exist mainly between −1.5 to 0 eV, and we will focus on them when making the comparison between DFT, DFT + U, and ARPES spectra next. The ARPES spectra[33] we make reference to in Fig. 8 are to our knowledge the latest and probably the best experimental data of such kind so far. Yet they still do not reach the resolution that can differentiate the six bands without ambiguity and are also contaminated by surface states. By projecting their DFT-calculated bands of bulk αU onto the (001) plane, Ref. 33 identified some possible surfaces, which are marked in Fig. 8 with shaded areas. It should be noted that those intensive spectrum features between −1.3 and −2.3 eV along Δ-Υ are not among such states. We nevertheless doubt that some of them may still be artificial, especially those below −1.6 eV where the corresponding DOS is quite flat. Despite all the above imperfections, we can get the following key conclusion from band structure results in Fig. 8: bands I–IV around Γ from DFT + U are shifted upward by about 0.1 eV or more with respect to DFT. The effect is most obvious for band I around Γ (marked with two green arrows), above which some ARPES spectrum features happen to exist. The upward shifting brings calculated band I closer to these spectra, which is consistent with what happens for peak I of DOS in the right panel of Fig. 8.

Overall, Fig. 8 shows that DFT + U at $U_{\text{eff}} = 1.24$ eV obtains better electronic structure for αU than DFT by shifting upward and intensify some f states directly below Fermi level, which we argue is the underlying mechanism that leads to the improvement in the calculated energetics and volume shown above.

Figure 8 also provides some insights on the relativistic effect of SOC. In terms of DOS, the intensity of peak I increases, peak II decreases, and peak III also increases due to SOC (the increasing/decreasing is illustrated with the directions of the arrows in Fig. 8). The effect seems most pronounced for peak I from the DFT + U calculation (compare red solid and red dashed peak I). The positions of these peaks, however, almost stay the same. Not surprisingly, Fig. 8 also shows that there is no significant shifting or splitting of bands due to SOC below Fermi level. In general, there is only a small difference between noSOC and SOC in the calculated DOS in the occupied part of the valence band shown in Fig. 8, which is in agreement with the previous study by FPLMTO.[16] The major effect of SOC that leads to the slight improvement in calculated properties for αU is to adjust the intensity of electronic states. The adjustment is small, and hence the improvement is also not large, about 0.02 eV/atom in terms of enthalpy, as we have found above.

Next we look at the full valence band of αU in Fig. 9. Here instead of the UPS spectra from Ref. 32 that is used above, we use the x-ray photoemission (XPS) and the Bremsstrahlung isochromat spectroscopy (BIS) spectra from Ref. 93 as the experimental references. They have both been properly normalized, so we can also compare the peak intensity as well. The major features of αU's valence band from XPS and BIS spectra are the three peaks near −0.3, 0.4 and 2.3 eV, respectively. The first one is peak I, discussed above; the latter two will be referred to as peak A and peak B, respectively.

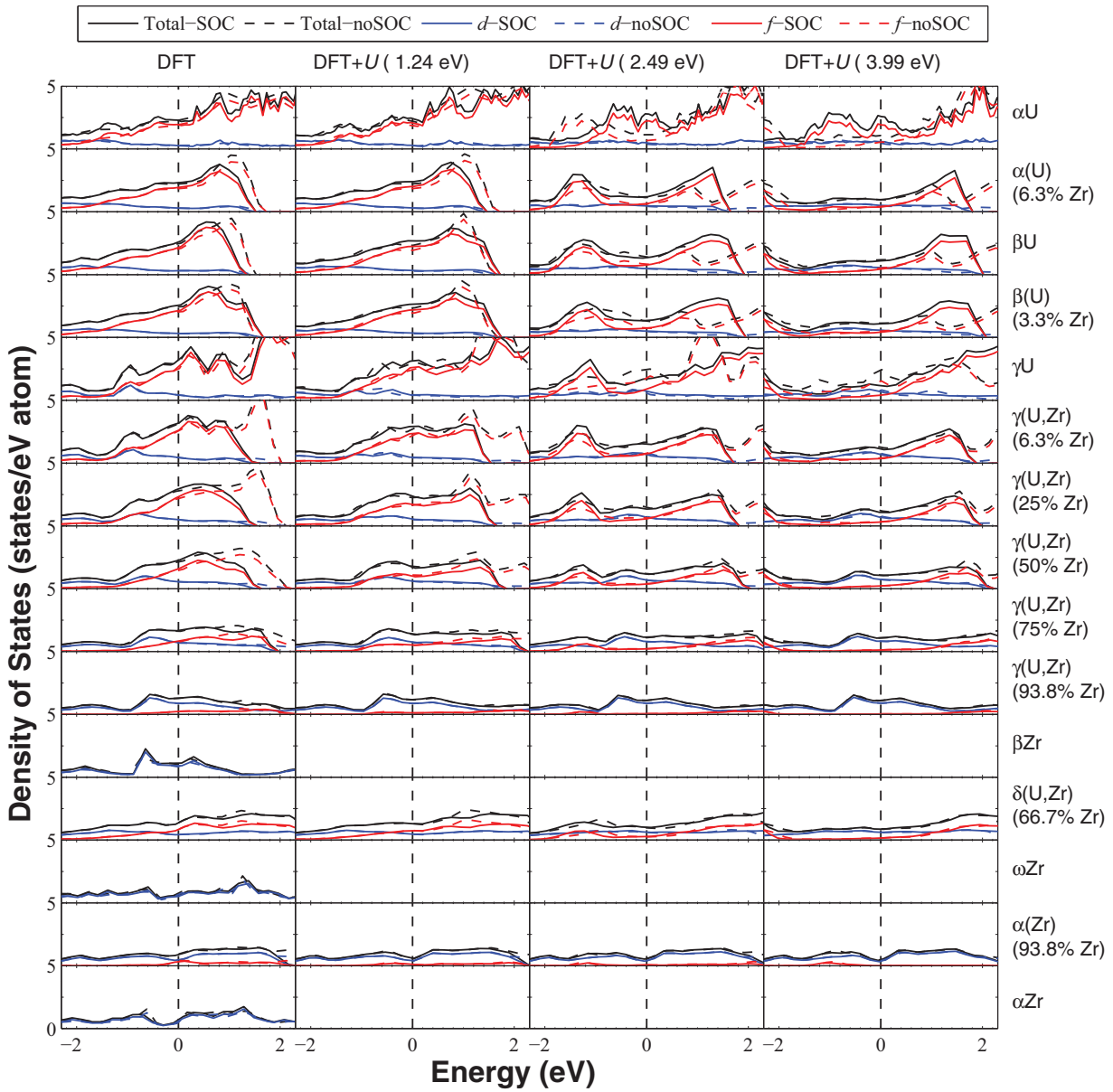

FIG. 10. (Color online) Total, $d-$ and f-orbital projected densities of state for all solid phases of U, Zr metal, and U-Zr alloy as functions of U_{eff}. The vertical dashed reference line is Fermi level. The first column is calculated by DFT and the second, third, and fourth by DFT + U at $U_{\text{eff}} = 1.24$, 2.49, and 3.99 eV, respectively. Results from both noSOC (dashed curves) and SOC (solid curves) are given. The highest unoccupied part of the valence band is missing for some systems due to limited number of bands included in the calculations.

Above Fermi level, peak A was suggested[94] to be the $5f_{5/2}$ subshell and peak B the $5f_{7/2}$ subshell. Note peak B should be further split into two subpeaks, as seen in the DOS from our calculations and the previous ones by FPLAPW.[94] Such a feature is not resolved in the BIS spectra, probably due to the core-hole lifetime broadening of about 1 eV.[94] Now we discuss our calculated results and compare them to the XPS/BIS spectra. First, going from DFT to DFT + U at $U_{\text{eff}} = 1.24$ eV in SOC calculations (i.e., going from the first to the second row on the right column), peak I slightly shifts upward and becomes higher but narrower, as has been shown more clearly in Fig. 8; peak A becomes higher and narrower as well but shifts downward, by a much larger extent than that of peak I; peak B also evolves in similar ways. All these changes are toward better agreement with the measured XPS/BIS spectra, which are similar to the results when going from DFT-LDA to QSGW.[34]

Next, we discuss the effect of SOC by comparing the left and the right column of the first (i.e., DFT) or second (i.e., DFT + U at $U_{\text{eff}} = 1.24$ eV) row. Again we focus on the unoccupied part. On the left (i.e, noSOC), peak A and the left subpeak of B are mixed/overlapped, which together make a single peak near 1 eV. In comparison, on the right, peak A and the left subpeak of peak B are separate, which are near 0.7 and 1.5 eV, respectively. Such splitting is the so-called spin-orbit splitting. The spin-orbit splitting of about 0.8 eV

is consistent with the literature value of 0.77 eV.[95] The extent of splitting is related to the spin-orbit coupling parameter, which for neutral U atom has been measured experimentally to be 0.22 eV (1773 cm^{-1}).[96] Finally, as previous studies[16,34] suggested, correlation and relativistic effects predominate in the unoccupied part, which is clearly seen in our results, in that the relative extent of improvement (e.g., peak shifts) in the unoccupied part (i.e., peaks A and B) is much larger than that of the occupied part (i.e, peak I) when going from DFT to DFT + U at 1.24 eV and from noSOC to SOC.

Another main point of Fig. 9 is to demonstrate the evolution of DOS as a function of U_{eff}. From 0 to 1.24 eV, peaks evolve and change their positions and shapes, but the up and down spin lobes are still mostly overlapped. At 2.49 eV, the two spin lobes are split apart and no longer overlap. This corresponds to the emergence of spin magnetic moments, as we show in Fig. 7. Such splitting is large enough that the positions and shapes of the DOS peaks already deviate substantially from the experimental spectra. From 2.49 eV to 3.99 eV, the two spin lobes are split further apart. Especially in those from noSOC calculations at 3.99 eV (bottom left panel); there even is a gap open between the up and down spin channels of the f band, although overall, the valence band is still continuous across the Fermi level, and the system remains metallic. Based on the evolution of DOS, we can characterize the three stages constantly observed in the evolution of calculated properties as functions of U_{eff}; roughly, they are metal, metal-gap transition, and gap stages, where the gap refers to splitting between the up and down spin channels of the f band. Overall, the comparison of calculated DOS with experimental spectra here align with those of energetics, volume, and magnetic moments above, which suggests that a reasonable U_{eff} should be smaller than 2.49 eV, and 1.24 eV seems a good choice.

Such a pattern for the change of DOS as a function of U_{eff} is actually quite similar for all solid phases of U metal and U-Zr alloy, as we can see in Fig. 10. Although the highest unoccupied part of the valence bands are not shown because they are not included in our calculations due to computing capability limits, the available data in Fig. 10 are enough to offer the following insights. First, slightly different from αU, in some systems, like α(U) (6.3 at.% Zr) and γU, the two $5f$ lobes already separate enough at $U_{\text{eff}} = 2.49$ eV to open a gap for the f band, although the whole valence band only shows a pseudo-gap because the d band (blue curves) stays essentially unchanged. The U_{eff}'s corresponding to the minimum in enthalpy or the second cross with the CALPHAD lines in Figs. 2 and 3 are in this region. Such a pseudo-gap should be unphysical for these metallic systems; hence, the U_{eff}'s should not be picked as the optimal U_{eff}. Moreover, the DOS curves in Fig. 10 also show the impact on U electronic properties upon alloying with Zr. No significant changes of the position and shape of the valence bands happen after U and Zr are alloyed. This phenomenon is most evident if we look at the DOS curves for γ(U,Zr) at various Zr concentrations between the sixth and the tenth rows in Fig. 10. They look quite like linear suppositions of the DOS curves for γU and βZr metal end members in the 5th and 11th rows. These trends show that alloying with Zr does not dramatically impact the qualitative U electronic structure, and therefore U-Zr alloy should have a similar correlation strength as U metal.

The total f-orbital occupation for U and U-Zr as a function of U_{eff} is shown in Fig. 11. First consider the magnitude of

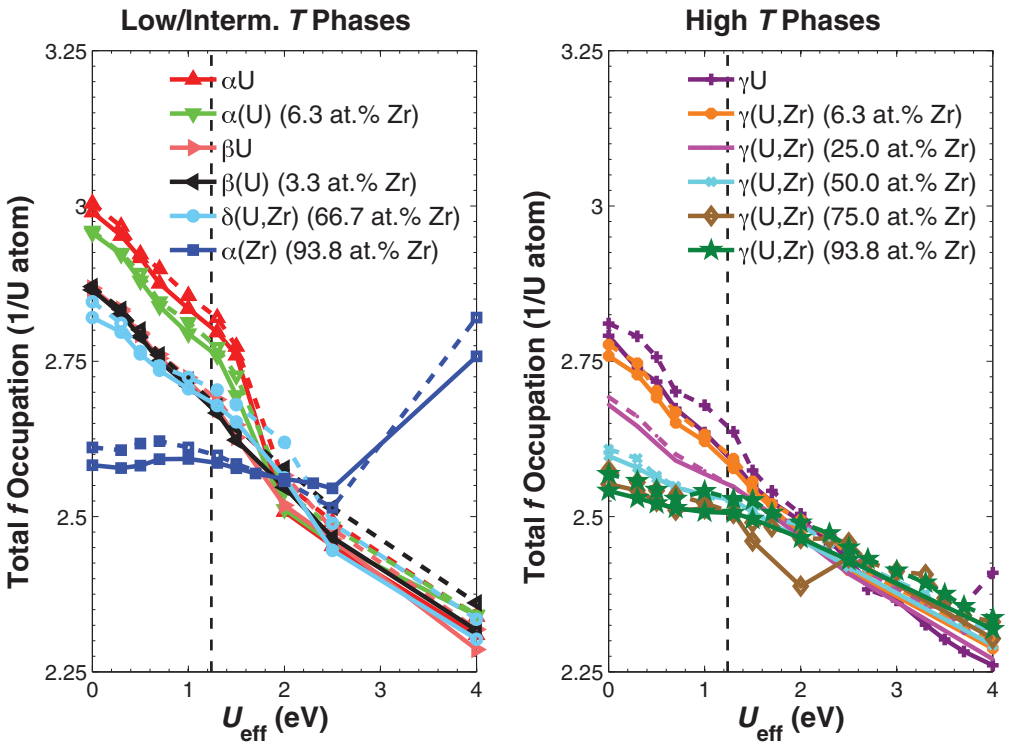

FIG. 11. (Color online) Total f-orbital occupation for all solid phases of U metal and U-Zr alloy as a function of U_{eff}. Low and intermediate temperature phases αU, α(U), βU, β(U), α(Zr), and δ(U,Zr) are plotted in the left panel; high temperature phases γU and γ(U,Zr) are in the right panel. Solid curves are from SOC calculations, while dashed curves are from noSOC.

the occupation as calculated by DFT. We point out beforehand that our values presented next are calculated using the quick projection scheme (LORBIT=11) implemented in VASP and are probably underestimated to some extent, possibly because the projection sphere radii are not sufficiently large. For the three allotropes of U metal—αU, βU to γU—the f-orbital occupation decreases consecutively from 3.01 to 2.87 and 2.81, respectively. Chantis *et al.*[34] obtained an αU f-orbital occupation of 3.57 and 3.19, respectively, from DFT-LDA and QSGW calculations. Our DFT-GGA calculation is 3.01 due to the projection issue. The U atom has three f electrons in the ground atomic state;[97] in crystal it should have fewer than three due to hybridization with other orbitals such as $6d$. Despite the projection issue, our DFT calculations still get a value larger than 3 and hence repeat the previous observation[34] that DFT overestimates the f-orbital occupation for U metal. Alloying with Zr in general reduces the f-orbital occupation. The reduction is negligible when the Zr concentration is small. For example, at 3.3 at.% Zr, β(U)'s f-orbital occupation curves are almost indistinguishable from βU's. However, it becomes more significant when the Zr concentration gets higher. This is most evident if we look at γ(U,Zr), which has f-orbital occupations of 2.78, 2.69, 2.60, 2.57, and 2.57 at 6.3, 25.0, 50.0, 75.0, and 93.8 at.% Zr, respectively, suggesting that at a higher Zr concentration, the f orbitals of U have stronger hybridization with Zr. Second, Fig. 11 also shows that, like QSGW, DFT + U reduces f-orbital occupation relative to DFT for all the systems considered, which serves as more evidence that it models the correlation effects better. These lost charges can be due to the hybridization of f orbitals with other orbitals of U atoms, which is presumably the only mechanism for U metal. For U-Zr alloy, f orbitals can also hybridize with orbitals of Zr atoms—mostly d orbitals, as evidenced by the slightly increased d-orbital occupation of Zr (not shown in Fig. 11). Third, SOC also reduces the occupation when U_{eff} is in the reasonable range of <2 eV (i.e., the dashed curves from noSOC are generally above the solid curves from SOC in this region); the change is marginally small, on the order of 0.001. Finally, for most systems, the total $f-$orbital occupation decreases in the whole $U_{\text{eff}} = 0$–4 eV range, and there seems to be a slight change of slope near $U_{\text{eff}} = 2$ eV. However, for α(Zr) at 93.8 at.% Zr, the occupation starts to recover at U_{eff} near 2.5 eV. We point out this is probably not an anomaly because, in a few systems, we also perform calculations that go beyond $U_{\text{eff}} = 4$ eV and find that their total f occupation also goes up at some higher U_{eff}. Therefore, total f occupation can also be considered to evolve in three stages as a function of U_{eff}. In general, Fig. 11 suggests that the total f occupation is a good parameter to characterize the correlation effects and how well they are modeled.

Summarizing all the fitting results above suggests that a good empirical U_{eff} for U and U-Zr should be between 1 and 1.5 eV, with the statistical optimal from energetic fitting to be 1.24 eV. How does it compare to theoretical Hubbard U? Herbst *et al.* estimated based on relativistic Hartree-Fock-Wigner-Seitz band calculations that the Hubbard U for U metal is $\sim$2 eV.[98] Table V gives that our calculation based on the linear response approach (Ref. 43) obtains theoretical U that goes from 1.87 eV for αU to 2.34 eV for γ(U,Zr) at 50 at.%Zr. Note that correlation is normally characterized by the ratio U/W, where U is the Hubbard U and W is the valence band width. Therefore, an appropriate energy scale to characterize the magnitude of U is $\sim$4 eV, which is W for αU. The comparison shows that theoretical U's are close to but larger than the empirical U_{eff} by 0.63 to 1.1 eV, or 16 to 28% W. This result is not surprising because DFT + U is based on the Hartree-Fock method, which is known to overestimate spin/orbital polarization; therefore, in real calculations, a smaller U_{eff} should be used to compensate the effect. The difference suggests that (1) it may not be optimal to use theoretical U directly in DFT + U calculations of U and U-Zr, and (2) theoretical Us are still reasonably close to and can definitely provide guidelines for the empirical U_{eff}. Moreover, Table V also illustrates the important point that there is only a small change in the Hubbard U for uranium between different phases and at different compositions of U and U-Zr. Among different phases, for example, αU, βU, and γU have theoretical U values of 1.87, 2.10, and 2.10 eV, respectively, and the span is 0.23 eV, or 6% of W. The effect of composition is best illustrated when we look at the bcc phases, γU, and γ(U,Zr). We see that when going from 0 to 93.75 at.% Zr, U reaches a maximum of 2.34 eV at 50 at.% Zr, which is about 0.24 eV higher than the minimum at 0 at.% Zr, or 6%W again. The small variations in U suggest that we may use a single U_{eff} for DFT + U calculations of U and U-Zr. Based on our study, we suggest the use of $U_{\text{eff}} = 1.24$ eV. Its magnitude is much smaller than that for U oxides like UO_2, for which Ref. 42 suggests the empirical U_{eff} to be 3 eV. Finally, we finish our discussion with two comments regarding U_{eff} for U and U-Zr: (1) We emphasize that although we have checked many properties including energy, volume, and electronic structure etc., such an empirical U_{eff} value of 1.24 eV is chosen based primarily on fitting in energy, which means that it will serve best in calculating energetics (e.g., phase stability, defect formation energy, diffusion barriers etc.), and it may or may not be equally optimal for other properties like magnetic moments as well. (2) The difference between the magnitude of U_{eff} for U metal and that for UO_2 oxide agrees with the difference between their correlation strengths: U is a weakly to moderately correlated metal, while

TABLE V. Theoretical Hubbard U for uranium in all solid phases of U metal and U-Zr alloy evaluated with the linear response approach of Ref. 43.

Phase	Composition (at.% Zr)	Hubbard U (eV)
αU	0	1.87
α(U)	6.3	1.95
βU	0	2.10
β(U)	3.3	2.20
γU	0	2.10
	6.3	2.15
	25.0	2.27
γ(U,Zr)	50.0	2.34
	75.0	2.20
	93.8	2.15
δ(U,Zr)	66.7	2.21
α(Zr)	93.8	2.33

UO_2 is a strongly correlated Mott-Hubbard insulator. They also align with the degree of DFT + U's improvement over DFT: for U metal, the improvement is quantitative (slight shifting of band positions below Fermi level), while for UO_2 oxide, it is qualitative (opening the band gap).

IV. CONCLUSIONS

We have explored the correlation and relativistic effects in U metal and U-Zr alloy. All solid phases of U metal and U-Zr alloy have been studied in both DFT and DFT + U calculations without and with SOC included using the effective Hubbard U parameter, U_{eff}, ranging from 0 to 4 eV.

DFT overestimates the formation energetics of phases relative to the stable end-members by 0.10 and 0.07 eV/atom without and with SOC compared to established CALPHAD models; DFT + U improves the energetics, which matches CALPHAD at $U_{\text{eff}} = 1$–1.5 eV. A statistically best agreement is found at $U_{\text{eff}} = 1.24$ eV, with which DFT + U reduces the error to 0.04 and 0.02 eV/atom without and with SOC, respectively. Our validated DFT + U approach predicts that the bcc solution phase γ(U,Zr) only has a weakly positive and asymmetric mixing enthalpy, quite different from DFT and previous CALPHAD results, but consistent with a latest CALPHAD model.

Besides energetics, DFT also underestimates volume, misplaces bands immediately below Fermi level, and overestimates f-orbital occupation, while DFT + U with $U_{\text{eff}} = 1$–1.5 eV consistently improve all these properties and, in general, still neither promotes ordered magnetic moments nor opens unphysical band gaps, consistent with the experimental results.

The calculated properties in general evolve as functions of U_{eff} in three stages roughly corresponding to metal, metal-gap transition, and gap states, where the gap refers to splitting between the up and down spin channels of f bands.

The empirical U_{eff} values of 1–1.5 eV are close to but smaller than the theoretical estimation of 1.9–2.3 eV that we obtain from the linear response approach. U_{eff} is found to vary only slightly between different phases and at different compositions of U and U-Zr; thus, a single $U_{\text{eff}} = 1.24$ eV, which is the statistical optimal from energetic fitting, is suggested for both U and U-Zr.

The relativistic effect of SOC is found to lower energy by 0.02 eV/atom, increase volume by $<0.5\%$, adjust intensities of states below Fermi level and split bands above it, and very slightly reduce the f-orbital occupation. It predominates in the unoccupied part of the valence band, so the effect on all these calculated ground state properties is small.

Finally, alloying with Zr generally reduces the f-orbital occupation and increases the Hubbard U slightly but does not change the qualitative features of valence bands. U-Zr alloy therefore should have strengths of correlation similar to U metal.

ACKNOWLEDGMENTS

This research is funded by the US Department of Energy Office of Nuclear Energy's Nuclear Energy University Programs under Contract No. 00088978. We acknowledge computing time from Idaho National Laboratory's Center for Advanced Modeling and Simulation and also from TeraGrid resources provided by Texas Advanced Computing Center under Grant No. [TG-DMR090023]. We thank C. Shen, Austin Y. Chang, Y. Lee, A. Bengtson, N. Pinney, D. Shrader, M. Gadre, and F. Zhou and CompuTherm LLC for various help during this research.

*weixie4@gmail.com
†ddmorgan@wisc.edu

[1] G. L. Hofman, L. C. Walters, and T. H. Bauer, Prog. Nucl. Energy **31**, 83 (1997).
[2] F. L. Oetting, M. H. Rand, E. F. J. Westrum, I. A. E. Agency, and V. A. Medvedev, *The Chemical Thermodynamics of Actinide Elements and Compounds: Part 1 The Actinide Elements* (International Atomic Energy Agency, Vienna, Austria, 1976).
[3] P. Chiotti, V. Akhachinskij, I. Ansara, and M. Rand, *The Chemical Thermodynamics of Actinide Elements and Compounds: Part 5, The Actinide Binary Alloys* (International Atomic Energy Agency, Vienna, Austria, 1981).
[4] R. I. Sheldon and D. E. Peterson, Bull. Alloy Phase Diagrams **10**, 165 (1989).
[5] G. H. Lander, E. S. Fisher, and S. D. Bader, Adv. Phys. **43**, 1 (1994).
[6] P. Soderlind, Adv. Phys. **47**, 959 (1998).
[7] P. Hohenberg and W. Kohn, Phys. Rev. **136**, B864 (1964).
[8] W. Kohn and L. J. Sham, Phys. Rev. **140**, A1133 (1965).
[9] H. L. Skriver, O. K. Andersen, and B. Johansson, Phys. Rev. Lett. **41**, 42 (1978).
[10] P. Soderlind, O. Eriksson, B. Johansson, and J. M. Wills, Phys. Rev. B **50**, 7291 (1994).
[11] J. Akella, S. Weir, J. M. Wills, and P. Soderlind, J. Phys.: Condens. Matter **9**, L549 (1997).
[12] L. Vitos, J. Kollár, and H. L. Skriver, J. Alloys Compd. **271**, 339 (1998).
[13] J. C. Boettger, M. D. Jones, and R. C. Albers, Int. J. Quantum Chem. **75**, 911 (1999).
[14] M. D. Jones, J. C. Boettger, R. C. Albers, and D. J. Singh, Phys. Rev. B **61**, 4644 (2000).
[15] L. Nordstrom, J. M. Wills, P. H. Andersson, P. Soderlind, and O. Eriksson, Phys. Rev. B **63**, 035103 (2000).
[16] P. Soderlind, Phys. Rev. B **66**, 085113 (2002).
[17] M. Penicaud, J. Phys.: Condens. Matter **12**, 5819 (2000).
[18] M. Penicaud, J. Phys.: Condens. Matter **14**, 3575 (2002).
[19] C. D. Taylor, Phys. Rev. B **77**, 094119 (2008).
[20] J. H. Li, Q. B. Ren, C. H. Lu, L. Lu, Y. Dai, and B. X. Liu, J. Alloys Compd. **516**, 139 (2012).
[21] S. Adak, H. Nakotte, P. F. de Chatel, and B. Kiefer, Physica B **406**, 3342 (2011).
[22] S. K. Xiang, H. C. Huang, and L. M. Hsiung, J. Nucl. Mater. **375**, 113 (2008).
[23] B. Beeler, B. Good, S. Rashkeev, C. Deo, M. Baskes, and M. Okuniewski, J. Phys.: Condens. Matter **22**, 505703 (2010).

[24]B. Beeler, B. Good, S. Rashkeev, C. Deo, M. Baskes, and M. Okuniewski, J. Nucl. Mater. **425**, 2 (2012).
[25]B. Beeler, C. Deo, M. Baskes, and M. Okuniewski, J. Nucl. Mater. **433**, 143 (2013).
[26]D. C. Langreth and J. P. Perdew, Phys. Rev. B **21**, 5469 (1980).
[27]A. Landa, P. Soderlind, and P. E. A. Turchi, J. Alloys Compd. **478**, 103 (2009).
[28]G. Y. Huang and B. D. Wirth, J. Phys.: Condens. Matter **23**, 205402 (2011).
[29]G. Y. Huang and B. D. Wirth, J. Phys.: Condens. Matter **24**, 415404 (2012).
[30]C. B. Basak, S. Neogy, D. Srivastava, G. K. Dey, and S. Banerjee, Philos. Mag. **91**, 3290 (2011).
[31]M. Kurata, T. Ogata, K. Nakamura, and T. Ogawa, J. Alloys Compd. **271**, 636 (1998).
[32]C. P. Opeil, R. K. Schulze, M. E. Manley, J. C. Lashley, W. L. Hults, R. J. Hanrahan, Jr., J. L. Smith, B. Mihaila, K. B. Blagoev, R. C. Albers, and P. B. Littlewood, Phys. Rev. B **73**, 165109 (2006).
[33]C. P. Opeil, R. K. Schulze, H. M. Volz, J. C. Lashley, M. E. Manley, W. L. Hults, R. J. Hanrahan, Jr., J. L. Smith, B. Mihaila, K. B. Blagoev, R. C. Albers, and P. B. Littlewood, Phys. Rev. B **75**, 045120 (2007).
[34]A. N. Chantis, R. C. Albers, M. D. Jones, M. van Schilfgaarde, and T. Kotani, Phys. Rev. B **78**, 081101 (2008).
[35]Z. Fisk, J. L. Smith, H. R. Ott, and B. Batlogg, J. Magn. Magn. Mater. **52**, 79 (1985).
[36]V. I. Anisimov, F. Aryasetiawan, and A. I. Lichtenstein, J. Phys.: Condens. Matter **9**, 767 (1997).
[37]A. B. Shick and W. E. Pickett, Phys. Rev. Lett. **86**, 300 (2001).
[38]A. N. Yaresko, V. N. Antonov, and P. Fulde, Phys. Rev. B **67**, 155103 (2003).
[39]A. N. Yaresko, V. N. Antonov, and B. N. Harmon, Phys. Rev. B **68**, 214426 (2003).
[40]V. N. Antonov, B. N. Harmon, and A. N. Yaresko, Phys. Rev. B **68**, 214424 (2003).
[41]V. N. Antonov, B. N. Harmon, O. V. Andryushchenko, L. V. Bekenev, and A. N. Yaresko, Phys. Rev. B **68**, 214425 (2003).
[42]J. G. Yu, R. Devanathan, and W. J. Weber, J. Phys.: Condens. Matter **21**, 435401 (2009).
[43]M. Cococcioni and S. de Gironcoli, Phys. Rev. B **71**, 035105 (2005).
[44]C. S. Barrett, M. H. Mueller, and R. L. Hitterman, Phys. Rev. **129**, 625 (1963).
[45]A. C. Lawson, C. E. Olsen, J. W. J. Richardson, M. H. Mueller, and G. H. Lander, Acta Crystallogr. B **44**, 89 (1988).
[46]A. S. Wilson and R. E. Rundle, Acta Crystallogr. **2**, 126 (1949).
[47]J. Goldak, L. T. Lloyd, and C. S. Barrett, Phys. Rev. **144**, 478 (1966).
[48]J. C. Jamieson, Science **140**, 72 (1963).
[49]A. Heiming, W. Petry, J. Trampenau, W. Miekeley, and J. Cockcroft, J. Phys.: Condens. Matter **4**, 727 (1992).
[50]J. G. Huber and P. H. Ansari, Physica B + C **135**, 441 (1985).
[51]M. Akabori, A. Itoh, T. Ogawa, F. Kobayashi, and Y. Suzuki, J. Nucl. Mater. **188**, 249 (1992).
[52]A. Zunger, S. H. Wei, L. G. Ferreira, and J. E. Bernard, Phys. Rev. Lett. **65**, 353 (1990).
[53]A. van de Walle, M. Asta, and G. Ceder, Calphad **26**, 539 (2002).
[54]C. Jiang, C. Wolverton, J. Sofo, L. Q. Chen, and Z. K. Liu, Phys. Rev. B **69**, 214202 (2004).
[55]G. Kresse and J. Hafner, Phys. Rev. B **47**, 558 (1993).
[56]G. Kresse and J. Furthmuller, Phys. Rev. B **54**, 11169 (1996).
[57]P. E. Blochl, Phys. Rev. B **50**, 17953 (1994).
[58]G. Kresse and D. Joubert, Phys. Rev. B **59**, 1758 (1999).
[59]J. P. Perdew, K. Burke, and M. Ernzerhof, Phys. Rev. Lett. **77**, 3865 (1996).
[60]H. J. Monkhorst and J. D. Pack, Phys. Rev. B **13**, 5188 (1976).
[61]M. Methfessel and A. T. Paxton, Phys. Rev. B **40**, 3616 (1989).
[62]O. Bengone, M. Alouani, P. Blochl, and J. Hugel, Phys. Rev. B **62**, 16392 (2000).
[63]A. I. Liechtenstein, V. I. Anisimov, and J. Zaanen, Phys. Rev. B **52**, R5467 (1995).
[64]S. L. Dudarev, G. A. Botton, S. Y. Savrasov, C. J. Humphreys, and A. P. Sutton, Phys. Rev. B **57**, 1505 (1998).
[65]B. Dorado, B. Amadon, M. Freyss, and M. Bertolus, Phys. Rev. B **79**, 235125 (2009).
[66]B. Meredig, A. Thompson, H. A. Hansen, C. Wolverton, and A. van de Walle, Phys. Rev. B **82**, 195128 (2010).
[67]J. W. Ross and D. J. Lam, Phys. Rev. **165**, 617 (1968).
[68]G. H. Lander and M. H. Mueller, Acta Crystallogr. B **26**, 129 (1970).
[69]L. Kleinman, Phys. Rev. B **21**, 2630 (1980).
[70]A. H. Macdonald, W. E. Pickett, and D. D. Koelling, J. Phys. C. **13**, 2675 (1980).
[71]P. Soderlind, B. Grabowski, L. Yang, A. Landa, T. Bjorkman, P. Souvatzis, and O. Eriksson, Phys. Rev. B **85**, 060301 (2012).
[72]C. Kittel, *Introduction to Solid State Physics* (Wiley, Hoboken, NJ, 2005).
[73]Y. A. Chang, S. L. Chen, F. Zhang, X. Y. Yan, F. Y. Xie, R. Schmid-Fetzer, and W. A. Oates, Prog. Mater. Sci. **49**, 313 (2004).
[74]W. Xiong, W. Xie, C. Shen, and D. Morgan, J. Nucl. Mater. **443**, 331 (2013).
[75]M. Kurata, IOP Conf. Ser.: Mater. Sci. Eng. **9**, 012022 (2010).
[76]P. Y. Chevalier, E. Fischer, and B. Cheynet, Calphad **28**, 15 (2004).
[77]A. T. Dinsdale, Calphad **15**, 317 (1991).
[78]K. Nagarajan, R. Babu, and C. K. Mathews, J. Nucl. Mater. **203**, 221 (1993).
[79]G. B. Fedorov and E. A. Smirnov, At. Energ. **21**, 837 (1966).
[80]Y. Wang, S. Curtarolo, C. Jiang, R. Arroyave, T. Wang, G. Ceder, L. Q. Chen, and Z. K. Liu, Calphad **28**, 79 (2004).
[81]P. E. A. Turchi, I. A. Abrikosov, B. Burton, S. G. Fries, G. Grimvall, L. Kaufman, P. Korzhavyi, V. R. Manga, M. Ohno, A. Pisch, A. Scott, and W. Q. Zhang, Calphad **31**, 4 (2007).
[82]G. Grimvall, B. Magyari-Kope, V. Ozolins, and K. A. Persson, Rev. Mod. Phys. **84**, 945 (2012).
[83]S. Bajaj, A. Landa, P. Soderlind, P. E. A. Turchi, and R. Arroyave, J. Nucl. Mater. **419**, 177 (2011).
[84]A. Berche, N. Dupin, C. Gueneau, C. Rado, B. Sundman, and J. C. Dumas, J. Nucl. Mater. **411**, 131 (2011).
[85]V. L. Moruzzi, J. F. Janak, and K. Schwarz, Phys. Rev. B **37**, 790 (1988).
[86]T. Le Bihan, S. Heathman, M. Idiri, G. H. Lander, J. M. Wills, A. C. Lawson, and A. Lindbaum, Phys. Rev. B **67**, 134102 (2003).
[87]See Supplemental Material at http://link.aps.org/supplemental/10.1103/PhysRevB.88.235128 for a critical review of experimental structural data for U metal and datails of the Debye-Gruneisen quasiharmonic volume correction.

[88]P. Soderlind, L. Nordstrom, L. Yongming, and B. Johansson, Phys. Rev. B **42**, 4544 (1990).
[89]A. Jain, G. Hautier, C. J. Moore, S. P. Ong, C. C. Fischer, T. Mueller, K. A. Persson, and G. Ceder, Comput. Mater. Sci. **50**, 2295 (2011).
[90]L. F. Bates and D. Hughes, Proc. Phys. Soc. Lond, B **67**, 28 (1954).
[91]E. R. Ylvisaker, W. E. Pickett, and K. Koepernik, Phys. Rev. B **79**, 035103 (2009).
[92]A. B. Shick, V. Drchal, and L. Havela, Europhys. Lett. **69**, 588 (2005).
[93]Y. Baer and J. K. Lang, Phys. Rev. B **21**, 2060 (1980).
[94]J. G. Tobin, K. T. Moore, B. W. Chung, M. A. Wall, A. J. Schwartz, G. van der Laan, and A. L. Kutepov, Phys. Rev. B **72**, 085109 (2005).
[95]M. S. S. Brooks, Physica B + C **130**, 6 (1985).
[96]N. Spector, Phys. Rev. A **8**, 3270 (1973).
[97]K. T. Moore and G. van der Laan, Rev. Mod. Phys. **81**, 235 (2009).
[98]J. F. Herbst, R. E. Watson, and I. Lindgren, Phys. Rev. B **14**, 3265 (1976).